AGU PUBLICATIONS

Geochemistry, Geophysics, Geosystems

RESEARCH ARTICLE

10.1002/2014GC005422

Key Points:
- Conditions of alteration in volcanic environments is deduced from minerals
- Mineral chemistry and isotopes are used to constrain water types
- Oxygen isotopes are used to constrain changes in climate

Supporting Information:
- Readme
- Tables S1 and S2

Correspondence to:
K. S. Panter,
kpanter@bgsu.edu

Citation:
Antibus, J. V., K. S. Panter, T. I. Wilch, N. Dunbar, W. McIntosh, A. Tripati, I. Bindeman, and J. Blusztajn (2014), Alteration of volcaniclastic deposits at Minna Bluff: Geochemical insights on mineralizing environment and climate during the Late Miocene in Antarctica, *Geochem. Geophys. Geosyst.*, *15*, 3258–3280, doi:10.1002/2014GC005422.

Received 16 MAY 2014
Accepted 28 JUL 2014
Accepted article online 31 JUL 2014
Published online 19 AUG 2014

Alteration of volcaniclastic deposits at Minna Bluff: Geochemical insights on mineralizing environment and climate during the Late Miocene in Antarctica

Joanne V. Antibus[1], Kurt S. Panter[1], Thomas I. Wilch[2], Nelia Dunbar[3], William McIntosh[3], Aradhna Tripati[4], Ilya Bindeman[5], and Jerzy Blusztajn[6]

[1]Department of Geology, Bowling Green State University, Bowling Green, Ohio, USA, [2]Department of Geological Sciences, Albion College, Albion, Michigan, USA, [3]New Mexico Institute of Mining and Technology, Socorro, New Mexico, USA, [4]Department of Earth, Planetary, and Space Sciences and Department of Atmospheric and Oceanic Sciences, Institute of the Environment and Sustainability, Institute of Geophysics and Planetary Physics, California Nanosystems Institute, University of California, Los Angeles, California, USA, [5]Department of Geological Sciences, University of Oregon, Eugene, Oregon, USA, [6]Department of Geology and Geophysics, Woods Hole Oceanographic Institution, Woods Hole, Massachusetts, USA

Abstract Secondary minerals in volcaniclastic deposits at Minna Bluff, a 45 km long peninsula in the Ross Sea, are used to infer processes of alteration and environmental conditions in the Late Miocene. Glassy volcaniclastic deposits are altered and contain phillipsite and chabazite, low to high-Mg carbonates, chalcedony, and clay. The $\delta^{18}O$ of carbonates and chalcedony is variable, ranging from -0.50 to 21.53‰ and 0.68 to 10.37‰, respectively, and δD for chalcedony is light (-187.8 to -220.6‰), corresponding to Antarctic meteoric water. A mean carbonate $^{87}Sr/^{86}Sr$ ratio of 0.70327 ± 0.0009 (1σ, $n = 12$) is comparable to lava and suggests freshwater, as opposed to seawater, caused the alteration. Minerals were precipitated at elevated temperatures (91 and 104°C) based on quartz-calcite equilibrium, carbonate ^{13}C-^{18}C thermometry (Δ_{47} derived temperature = 5° to 43°C) and stability of zeolites in geothermal systems (>10 to ~100°C). The alteration was a result of isolated, ephemeral events involving the exchange between heated meteoric water and glass during or soon after the formation of each deposit. Near-surface evaporative distillation can explain ^{18}O-enriched compositions for some Mg-rich carbonates and chalcedony. The $\delta^{18}O_{water}$ calculated for carbonates (-15.8 to -22.9‰) reveals a broad change, becoming heavier between ~12 and ~7 Ma, consistent with a warming climate. These findings are independently corroborated by the interpretation of Late Miocene sedimentary sequences recovered from nearby sediment cores. However, in contrast to a cold-based thermal regime proposed for ice flow at core sites, wet-based conditions prevailed at Minna Bluff; a likely consequence of high heat flow associated with an active magma system.

1. Introduction

The alteration of glass-rich volcaniclastic rocks (e.g., hyaloclastites) has been studied in order to understand the style and mode of eruption, the environment in which the materials are deposited, and postdepositional processes of alteration. The glass in hyaloclastite, or in any vitric-rich volcanic material, is thermodynamically unstable and readily hydrates and devitrifies at temperatures ≤200°C to form, in general order of occurrence (for mafic-intermediate rock compositions), palagonite, clay minerals (e.g., smectite, kaolinite), zeolites, and carbonates [*Fisher and Schmincke*, 1984; *Stroncik and Schmincke*, 2002]. The alteration is a globally significant process whose study has led to major constraints on geochemical cycles involving interaction between seawater and the oceanic crust [*Staudigel et al.*, 1995; *Walton and Schiffman*, 2003; *Walton et al.*, 2005] and the contributions of altered oceanic crust to mantle source reservoirs for volcanism [*Geldmacher and Hoernle*, 2000; *Kelly et al.*, 2006]. In addition, the hydrothermal alteration of terrestrial deposits by meteoric water has been used to better understand paleoenvironments and climate [*Dallai and Burgess*, 2011] with applications to the study of Mars [*Bishop et al.*, 2002; *Greenberger et al.*, 2012]. The geochemistry of secondary minerals, in particular zeolites and carbonates, formed in volcaniclastic deposits have been used to distinguish seawater from freshwater sources [*Böhlke et al.*, 1980; *Johnson and Smellie*, 2007] and to better understand physiochemical conditions during alteration [*Jakobsson and Moore*, 1986; *Passaglia et al.*, 1990; *Révillon et al.*, 2007; *Renac et al.*, 2010].

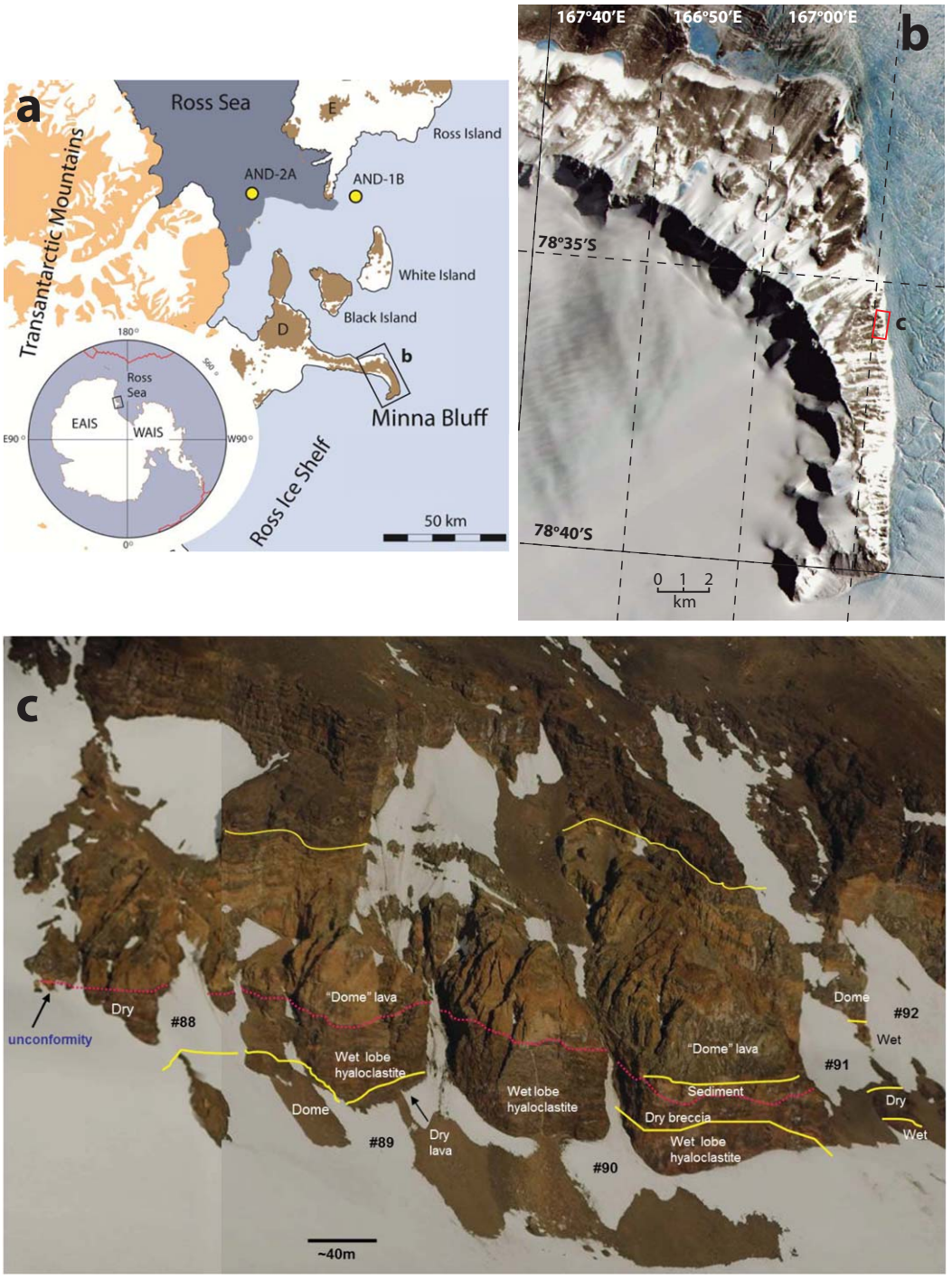

Figure 1. (a) Map of the McMurdo Sound region in the southern Ross Sea with areas of exposed Cenozoic volcanism (dark brown) including Minna Bluff peninsula, Mt. Discovery, D, and the currently active Mt. Erebus, E, located on Ross Island. ANDRILL core site locations (AND-1B and AND-2A) are shown. (b) ASTER satellite image of Minna Hook area at the southeastern end of the peninsula. (c) Composite aerial photograph of a well-exposed cliff section at Minna Hook that consists of alternating "dry" lava and breccia deposits with "wet" lobe hyaloclastite unconformably overlain by sediments and dome lavas.

Volcaniclastic deposits at Minna Bluff, a 45 km long volcanic peninsula extending southeast into the Ross Sea in Antarctica (Figure 1), provide an excellent opportunity to investigate conditions of alteration and to evaluate the use of secondary minerals as monitors of past environments. The deposits were formed in a variety of subaerial and subaqueous environments by direct volcanic activity or locally reworked by mass wasting, fluvial and glacial events [*Wilch et al*., 2011]. Minna Bluff was active between the Late Miocene (~12 Ma) and the Early

Pliocene (~4 Ma), which coincides with a period of dynamic climate change [*Passchier et al.*, 2011; *Naish et al.*, 2009; *McKay et al.*, 2009; *Wilson et al.*, 2012]. In addition, Minna Bluff acted as a significant barrier to regional ice flow from the south [*Kyle*, 1981; *Denton and Marchant*, 2000; *Wilson and Demosthenous*, 2000; *Talarico and Sandroni*, 2009] and thus has played an important role in the glacial history of this region of Antarctica.

2. Geology of Minna Bluff

Field mapping, geochemistry, and $^{40}Ar/^{39}Ar$ geochronology document a complex history at Minna Bluff that includes over 200 eruptive episodes from numerous overlapping volcanic centers as well as at least four major hiatuses in volcanic activity. Volcanic centers which comprise the older (12–8 Ma) Minna Hook area at the southeastern end of the peninsula (Figure 1) are revealed in well-exposed cliff sections and consist of alternating lavas, volcaniclastic deposits, and domes ranging in composition from basanite to phonolite (*Panter et al.*, 2011). In contrast, basaltic scoria cones and associated lavas dominate the younger (8–4 Ma) central and northwestern portions of the Minna Bluff peninsula [*Wilch et al.*, 2011]. It is proposed that Minna Bluff first formed as an island (Minna Hook) followed by the migration of activity to the northwest forming the peninsula that terminates in an area that is now beneath the younger Mt. Discovery volcano (J. R. Ross et al., manuscripts in preparation, 2014).

The Minna Hook stratigraphic succession includes alternating deposits of subaerial and subaqueous lava and volcaniclastic lithofacies which are exposed in cliffs that rise from near sea level to over 1000 m elevation [*Wilch et al.*, 2011]. The subaerial lithofacies include abundant tabular 'a'ā lava and associated reddened autobreccia. The subaqueous lithofacies are characterized by quenched pillow or lobe-shaped lava and associated yellow to buff colored, variably palagonitized hyaloclastic breccia (Figure 2a). It has long been hypothesized that the subaqueous environment was created by volcano-generated glacial meltwater [e.g., *Wright-Grassham*, 1987]. Primary types of volcaniclastic rocks at Minna Bluff are dominated by autoclastic and hyaloclastic deposits, with minor pyroclastic deposits [cf. *White and Houghton*, 2006]. Rare epiclastic sediments occur as thin (typically $<$2 m thick) layers on unconformities within the primary volcanic sequences and consist of heterolithic mixtures of mildly recycled juvenile clasts and lithic volcanic clasts deposited by debris flow, fluvial and glacial events [*Wilch et al.*, 2011].

The stratigraphic transitions from subaqueous to subaerial lithofacies (i.e., passage zones) are not well defined and consist of a zone of rocks that exhibit both subaqueous and subaerial characteristics. Such ill-defined passage zones are typical of 'a'ā lava delta sequences, where 'a'ā lavas flow from a subaerial to a subaqueous meltwater lake environment [*Smellie et al.*, 2013]. The alternating subaqueous and subaerial stratigraphic pattern and lack of thick delta and subaqueous sequences suggest that the eruptions occurred beneath relatively thin ice cover or in contact with small rapidly drained ice sheets indicating a wet-based thermal regime [*Wilch et al.*, 2011; *Smellie et al.*, 2014]. The fact that hyaloclastites and other volcaniclastic deposits have limited vertical extent ($<$50 m) suggests that magma-water interactions during volcanic activity at Minna Bluff were relatively isolated, sporadic, and short-lived events.

The ages of the volcaniclastic deposits investigated in this study are based on $^{40}Ar/^{39}Ar$ geochronology [*Fargo*, 2009; *Wilch et al.*, 2011; J. R. Ross et al., manuscripts in preparation, 2014]. The dating was performed on mineral (sanidine and kaersutitic amphibole) and groundmass concentrated from lava lobes, pumice, and lava clasts within volcanoclastic deposits. There are three types of ages provided in Table 1: ages directly from the deposits ($n = 17$), ages bracketed between dated overlying and underlying deposits (designated by both a greater than and a less than age; $n = 6$), or ages that are from deposits situated either above or below a dated deposit (designated by either a greater than age or a less than age; $n = 18$). No ages are listed for four samples because these samples are from sequences that lack age constraint. These four undated samples presumably date to the 12–4 Ma time span of Minna Bluff eruptions. It is important to note that the samples used to directly date the volcanoclastic deposits are not the matrix samples used in this study to investigate alteration history, however, both matrix and dating samples were collected from the same volcanoclastic deposit.

3. Analytical Methods

3.1. Sample Selection and Microscopy

A total of 45 samples from Minna Bluff were evaluated in this study. Samples were selected based on the presence of secondary minerals as well as their spatial representation within the stratigraphy and time span

Figure 2. Examples of altered volcanoclastic deposits at Minna Bluff and their corresponding hand samples. (a and b) Hyaloclastite breccia with pillow lava; sample MB-07-013. (c and d) Mineralized breccia; sample MB-07-132. (e and f) Pumice-rich polymict breccia; sample MB-07-172. (g and h) Agglutinated monomict breccia; sample MB-06-567. Total length of ice axe in Figures 2a, 2e, and 2g is approximately 1 m. Scale bar in Figures 2b, 2d, 2f, and 2h is divided into 1 cm segments.

Table 1. Sample Description

Sample Number	Deposit Type	Deposit Age, Ma (±)[a]	Alteration[b]	Elevation (m asl)	Environment of Deposition
MB-06-515	Fine conglomerate	>9.55 (0.05), <10.40 (0.05)	c > ph	78	Subglacial fluvial on a glacial unconformity
MB-06-521	Hyaloclastic breccia	>9.55 (0.05), <10.40 (0.05)	ph > c	50	Subaqueous environment on glacial unconformity
MB-06-523	Hyaloclastic breccia	10.40 (0.05)	ph > c	50	Subaqueous volcanic
MB-06-529	Hyaloclastic breccia	9.53 (0.10)	ph > c	50	Subaqeous volcanic on a glacial unconformity
MB-06-531	Autoclastic breccia	9.70 (0.05)	c	115	Subaerial volcanic
MB-06-540	Clastic dike	no age data	c > chz	275	Ice-contact remobilized sedimentary deposit
MB-06-548	Subglacial till	>11.44 (0.05)	c > ph	83	Subglacial glacial deposition
MB-06-550	Hyaloclastic breccia	>11.44 (0.05)	ph > c	275	Subaqueous volcanic below a glacial unconformity
MB-06-554	Hyaloclastic breccia	11.44 (0.05)	c > ph (degraded)	275	Subaqueous volcanic
MB-06-560	Hyaloclastic breccia	8.79 (0.30)	ph > c	154	Subaqueous volcanic
MB-06-567	Autoclastic breccia	>8.79 (0.30)	c > chz	228	Subaerial volcanic
MB-06-581	Hyaloclastic breccia	>10.45 (0.04)	ph > c	136	Subaqueous volcanic
MB-06-593	Hyaloclastic breccia	9.11 (0.18)	ph > c	35	Subaqueous volcanic above glacial unconformity
MB-06-602	Pebbly sandstone	>11.60 (0.07), <11.97 (0.50)	ph > c	225	Subglacial fluvial on glacial unconformity
MB-06-605	Hyaloclastic breccia	11.60 (0.07)	ph > c	240	Subaqueous volcanic
MB-06-623	Autoclastic breccia	>8.96 (0.33), <9.92 (0.23)	chz > c > ph	300	Subaerial volcanic
MB-06-626	Hyaloclastic breccia	9.92 (0.23)	c > chz	300	Subaqueous volcanic
MB-06-656	Autoclastic breccia	<9.77 (0.09)	chz > c > ph, dk	270	Subaerial volcanic
MB-06-678	Hyaloclastic breccia	9.10 (0.05)	ph > chz, c, rhd	675	Subaqueous volcanic delta forests
MB-06-694	Autoclastic breccia	<11.58 (0.006)	chz > c	243	Subaerial volcanic just above subaqueous transition
MB-06-696	Hyaloclastic breccia	<11.58 (0.006)	ph > c	230	Subaqueous volcanic
MB-06-700	Autoclastic breccia	<11.58 (0.006)	ph > c > chz	240	Subaerial volcanic
MB-06-716	Autoclastic breccia	>11.68 (0.04)	c	60	Subaerial volcanic
MB-06-724	Hyaloclastic breccia	>11.65 (0.09), <11.72 (0.07)	ph, c > chz	85	Subaqueous volcanic
MB-06-775	Hyaloclastic breccia	<8.20 (0.06)	ph > c	448	Subaqueous volcanic
MB-06-801	Sandstone	no age data	ph > c	60	Subaqueous volcanic-sediment deposition
MB-06-808	Conglomerate	no age data	ph > c	50	Subaqueous volcanic-sediment deposition
MB-07-013	Hyaloclastic breccia	>9.04 (0.57), <9.85 (0.48)	chz, c > ph	704	Transitional subaqueous/subaerial volcanic
MB-07-069	Hyaloclastic breccia	5.74 (0.15)	ph, chz > c	348	Transitional subaqueous/subaerial volcanic
MB-07-102	Hyaloclastic breccia	>7.11 (0.35)	ph > c	198	Subaqueous volcanic
MB-07-106	Pyroclastic lapilli-tuff	<7.91 (0.50)	ph > c	505	Subaerial volcanic
MB-07-111	Hyaloclastic breccia	<7.91 (0.50)	ph> c > chz	335	Transitional subaqueous/subaerial volcanic
MB-07-118	Pyroclastic lapilli-tuff	10.01 (0.32)	c	624	Subaerial volcanic
MB-07-132	Lava flow breccia	>9.42 (0.13)	c, chd	517	Hyrdothermally altered subaerial volcanic
MB-07-135	Autoclastic breccia	9.14 (0.04)	c > chz	690	Subaerial volcanic
MB-07-148	Hyaloclastic breccia	5.84 (0.88)	chz > c	195	Transitional subaqueous/subaerial volcanic
MB-07-152	Hyaloclastic breccia	7.64 (0.23)	c	265	Sheared water-saturated vent complex
MB-07-156	Pyroclastic lapilli-tuff	7.64 (0.23)	ph > c	500	Subaerial volcanic
MB-07-172	Pyroclastic breccia	9.72 (0.003)	ph (degraded) > c, dk	819	Subaerial explosion breccia
MB-07-190	Hyaloclastic breccia	<7.89 (0.028)	c, sid	438	Transitional subaqueous/subaerial volcanic
MB-07-218	Hyaloclastic breccia	>7.45 (0.031)	chz > c	528	Subaqueous volcanic
MB-07-221	Lapilli-tuff	No age data	c > ph	396	Subaerial volcanic
MB-07-230	Lapilli-tuff	9.04 (0.57)	c	649	Subaerial volcanic vent complex
MB-07-234	Lapilli-tuff	<7.91 (0.50)	chz > c	691	Subaerial volcanic cone flank
MB-07-237	Lapilli-tuff	<7.91 (0.50)	ph > c	213	Subaerial volcanic

[a]Age based on 40Ar/39Ar dating [*Fargo*, 2009; *Wilch et al*., 2011[(*J. R. Ross et al*., manuscripts in preparation, 2014). Ages are based on dating the deposit or from dating stratigraphically lower or higher deposits, giving less than and/or greater than ages, respectively. The ages that directly date the deposits were determined on samples collected from the same deposit but are not the same samples used in this study. The precision of the ages are at one standard deviation (1σ) and correspond to the analytical and statistical errors on plateau age spectra or on the weighted mean age of selected heating steps.

[b]Relative abundance of secondary minerals: phillpsite (ph), chabazite (chz), carbonates (c), chalcedony (chd), dickite (dk), siderite (sd), and rhodochrosite (rhd).

relative to the total duration of volcanic activity at Minna Bluff (Table 1 and Figure 1). Twenty-three of the samples are classified as hyaloclastites, 15 are from other primary volcaniclastic deposits (e.g., autoclastic breccia, pyroclastic lapilli tuff), and 6 samples are from epiclastic deposits. The samples range from matrix supported to clast supported and include both monomictic and polymictic varieties (Figure 2). Clasts range from ash/sand to lapilli/pebble in size, have textures that range from aphanitic to porphyritic, and are nonvesicular to highly vesicular (scoriaceous; Figure 2).

Standard microscopic techniques were used to describe the lithology of the clasts and matrix, including a first-order identification of secondary minerals and their parageneses. Secondary minerals were formed in several open-space types, including vugs, fractures, vesicles, and intergranular voids. In this study, vugs in lava clasts are defined as large (>1.0 mm), irregular-shaped, partially to fully enclosed cavities. Vesicles are defined as smaller (<1.0 mm) cavities in lava clasts that are more spherical in shape. Intergranular voids

represent large, irregular opened spaces in the matrix between lava clasts. Fractures are mineral-filled cracks that cut through the matrix and in some instances bisect lava clasts.

Zeolite and clay minerals are identified through petrographic means as well as X-ray diffraction (XRD) analysis using a Bruker D8 Advance Series II at the Ohio State University. Material for XRD analysis was separated from the host rock, ground to 75 μm size, and step scanned at 0.05° interval and 4 s step time from 2 to 65° 2σ. Data were collected by XRD Commander software. The peak search/match routine was carried out on the raw, unprocessed pattern using EVA software and the ICDD PDF-2 Release 2009 powder diffraction database. Cathode luminescence (CL) analyses of carbonates were performed on polished thin sections using a cold cathode system on a petrographic microscope.

3.2. Mineral Chemistry

Major and minor elements for zeolites, carbonates, chalcedony, and dickite (clay) were determined from 24 polished sections (~50 μm thick) using the electron microprobe (EMP) facilities at the New Mexico Institute of Mining and Technology and the University of Michigan. A Cameca SX 100 EMPA was used at both facilities, and all minerals were analyzed using a 10 μm beam diameter and a standard suite of natural and synthetic silicate and carbonate minerals for calibration. Phillipsite and chabazite analyses used a beam current of 2–20 nA and counting times of 10–20 s. Carbonate analyses used a beam current of 4 nA and counting times of 5–30 s. Detection limits for EMP analyses varied with concentration between ±0.01 wt % (1σ) for elements measured at >20 wt % and ±0.1 wt % (1σ) for those with concentrations <5 wt %. Due to the hydrous nature of zeolites, subsolidus cation exchange between coexisting phases often occurs [*Deer et al*., 1966] and can modify the original composition. For this study, only zeolite analyses that have oxide totals greater than 87 wt % and [Al_2O_3/((Ca, Na_2, K_2, Mg) · O)] ratios equal to 1.0 (±0.07 1σ) [cf. *Deer et al*., 1966] are accepted (Table 2). Of the 24 samples analyzed for zeolites, 13 samples yield acceptable values for phillipsite (n = 63 spot analyses) and 9 samples yield acceptable values for chabazite (n = 36 spot analyses).

3.3. Isotopes

3.3.1. Oxygen and Carbon Isotopes on Carbonates

Carbonate phases were analyzed for oxygen and carbon isotopes at the University of Michigan. Aliquots for six samples were obtained using conventional drilling and seven additional samples were collected using a computerized Merchantek MicroMill, which allowed individual layers as small as 10 μm in width to be sampled. All powdered carbonate material was roasted under vacuum for 1 h at 200°C to remove any volatile contaminants and water. Carbonate material was reacted at 77 ± 1.0°C in four drops of anhydrous phosphoric acid for 8 min and processed on a triple collector gas source Finnigan MAT 253 mass spectrometer coupled to a Finnigan Kiel IV automated preparation device. Values for δ^{18}O are reported relative to V-SMOW and δ^{13}C values are reported relative to the V-PDB, both in per mil (‰). Precision for both δ^{18}O and δ^{13}C is ±0.1‰ or better as compared to the National Bureau standards NBS 18 and NBS 19.

Five of the samples were also analyzed using gas source mass spectrometers that have been specially modified for the analysis of multiply substituted isotopologs of CO_2 and are integrated with a fully automated systems for carbonate sample digestion in phosphoric acid, purification of the resultant CO_2, and introduction [*Eiler*, 2007; *Huntington et al*., 2009; *Tripati et al*., 2010]. Typically analyses of two unknown samples and three standards were performed each day. Both carbonate standards and "heated gases" were analyzed. Heated gases are composed of CO_2 with a stochastic distribution of isotopes between isotopologs. Gases with different bulk δ^{18}O and δ^{13}C ratios in quartz breakseals are heated to 1000°C for 2 h and then quenched at room temperature. These standard gases are then purified and analyzed using the same protocol as sample gases. Standards are also used for the calculation of sample Δ_{47} values, which is the parts per thousand excess of CO_2 isotopologs with a mass of 47 amu (as compared to 44 amu in a sample) and a hypothetical sample with same bulk isotope composition but a stochastic distribution of isotopes amongst all isotopologs of CO_2. Typical precision is 0.009‰ (1 s.e.), equivalent to about 2°C [*Eiler*, 2007; *Huntington et al*., 2009; *Tripati et al*., 2010] although better precision can be attained through the analysis of clean sample gases and extensive replication. The ^{13}C-^{18}O thermometer does not require prior knowledge of the concentration of ^{18}O in the water since the calculated parameter (Δ_{47}) is correlated to the inverse square of the temperature. Isotope ratios were determined both relative to a stochastic distribution [*Ghosh et al*., 2006] and on the absolute reference frame of *Dennis et al*. [2011] based on the analysis of water-equilibrated CO_2.

Table 2. Major Element Abundances of Representative Zeolites From Minna Bluff[a]

	Weight Percent Oxides										Cations per Formula Unit (Based on 32 Oxygens)									Molecular Ratio
Sample	SiO_2	TiO_2	Al_2O_3	MnO	MgO	FeO	CaO	Na_2O	K_2O	Total	Si	Ti	Al	Mn	Mg	Fe	Ca	Na	K	Al_2O_3/(Ca, Mg, Na, K)O
Phillipsite																				
MB-07–069-18	51.49	n.d.[a]	22.68	0.20	5.19	10.98	5.55	1.86	2.22	100.17	8.55	0.00	5.01	0.00	2.55	0.20	1.66	0.98	0.66	0.85
MB-07–069-19	41.80	n.d.	21.69	0.15	4.22	9.73	6.07	1.95	2.05	87.66	8.67	0.00	5.27	0.00	2.05	0.17	1.79	1.02	0.61	0.96
MB-07–069-27	48.74	n.d.	23.34	0.02	0.10	0.09	4.35	4.61	7.49	88.74	10.02	0.00	5.63	0.00	0.05	0.00	1.23	2.28	2.15	0.99
MB-07–148-06	57.76	0.05	25.90	n.d.	0.00	0.12	0.33	7.80	8.54	100.50	11.62	0.01	5.5	0.00	0.00	0.02	0.07	2.78	2.01	1.13
MB-07–148-27	61.39	0.03	22.11	n.d.	0.03	n.d.	0.09	6.63	9.72	100.00	11.24	0.00	4.78	0.00	0.00	0.00	0.02	2.36	2.27	1.03
MB-07–148-29	58.08	0.07	24.65	n.d.	n.d.	0.11	0.20	7.55	9.36	100.02	10.71	0.01	5.37	0.00	0.00	0.02	0.03	2.71	2.19	1.08
MB-06–775-18	57.17	n.d.	19.38	0.01	0.02	0.06	0.38	4.15	8.73	89.90	11.40	0.00	4.56	0.00	0.00	0.00	0.11	1.99	2.46	0.99
MB-06–775-19	60.92	n.d.	20.06	0.01	n.d.	0.03	0.21	3.98	8.88	94.09	11.50	0.00	4.43	0.00	0.00	0.00	0.06	1.89	2.50	0.99
MB-06–775-20	57.19	n.d.	19.38	n.d.	0.01	0.05	0.11	4.25	7.99	88.98	11.47	0.00	4.58	0.00	0.00	0.00	0.03	2.01	2.23	1.06
MB-07–102-35	55.66	n.d.	20.96	n.d.	0.04	0.11	0.70	4.21	7.47	89.15	11.14	0.00	4.92	0.00	0.02	0.00	0.19	2.19	2.11	1.09
MB-07–102-39	57.24	n.d.	23.30	n.d.	0.03	0.07	0.60	5.02	7.52	93.78	11.07	0.00	5.00	0.00	0.01	0.00	0.17	2.41	2.13	1.06
MB-07–102-40	56.70	n.d.	20.32	n.d.	0.01	0.07	0.53	4.90	7.66	90.19	11.25	0.00	4.74	0.00	0.01	0.00	0.14	2.36	2.16	1.02
MB-07–156-01	48.22	n.d.	24.44	0.01	0.01	0.24	0.79	4.81	9.79	88.31	10.03	0.00	5.96	0.00	0.00	0.00	0.22	2.51	2.85	1.06
MB-07–156-06	51.37	n.d.	23.45	n.d.	0.02	0.08	0.39	4.71	9.71	89.73	10.89	0.00	5.83	0.00	0.08	0.00	0.11	2.39	2.91	1.06
MB-07–156-07	53.28	n.d.	21.49	0.01	0.00	0.09	0.06	5.25	9.07	89.25	10.85	0.00	5.14	0.00	0.00	0.00	0.01	2.55	2.57	0.99
MB-06–529-2125	51.79	n.d.	20.94	n.d.	0.03	n.d.	0.11	6.19	8.86	87.92	10.76	0.00	5.14	0.00	0.01	0.00	0.03	3.05	2.56	0.91
MB-06–529-2126	53.28	n.d.	21.94	n.d.	0.02	n.d.	0.20	5.81	8.39	89.64	10.81	0.00	5.13	0.00	0.01	0.00	0.06	2.82	2.39	0.97
MB-06–529-2127	52.15	n.d.	21.53	n.d.	0.03	n.d.	0.11	5.88	8.31	88.01	10.77	0.00	5.23	0.00	0.01	0.00	0.03	2.86	2.38	0.99
MB-06–523-027	54.70	n.d.	20.20	n.d.	0.27	0.28	0.31	3.67	8.95	88.38	11.51	0.00	4.99	0.00	0.00	0.06	0.09	1.91	2.74	1.03
MB-06–523-2140	59.33	n.d.	20.63	n.d.	0.01	0.08	0.17	5.74	10.55	96.51	11.37	0.00	4.68	0.00	0.00	0.01	0.03	2.14	2.59	0.98
MB-06–696-01	61.92	0.05	22.56	0.02	0.01	0.08	0.42	5.49	9.45	100.00	11.29	0.01	4.82	0.00	0.00	0.01	0.08	1.97	2.19	0.98
MB-06–696-23	56.59	n.d.	19.37	n.d.	n.d.	0.03	0.23	5.39	10.25	91.86	11.32	0.00	4.62	0.00	0.00	0.01	0.06	2.01	2.62	1.00
MB-06–560-10	61.51	n.d.	21.36	n.d.	0.98	0.1	2.25	5.71	8.09	100.00	9.86	0.00	4.06	0.00	0.23	0.01	0.39	1.74	1.74	1.04
Chabazite																				
MB-06–626-14	55.98	n.d.	26.51	n.d.	n.d.	0.01	0.29	9.52	9.52	101.83	10.37	0.00	5.79	0.00	0.00	0.00	0.06	2.77	2.25	1.14
MB-06–626-31	54.69	n.d.	27.29	n.d.	n.d.	0.01	0.17	8.12	9.71	99.99	10.18	0.00	5.98	0.00	0.00	0.00	0.03	2.93	2.31	1.14
MB-06–656-12	52.77	n.d.	24.57	n.d.	n.d.	0.06	0.07	6.46	13.19	97.12	10.32	0.00	5.66	0.00	0.00	0.00	0.01	2.50	3.20	1.06
MB-06–656-13	53.34	n.d.	24.27	n.d.	n.d.	0.11	0.12	5.97	13.21	97.02	10.38	0.00	5.67	0.00	0.00	0.00	0.02	2.25	3.18	1.07
MB-06–656-14	54.09	n.d.	25.46	n.d.	n.d.	0.06	0.14	6.67	12.71	99.13	10.31	0.00	5.68	0.00	0.00	0.00	0.02	2.50	3.18	1.04
MB-06–550-05	56.70	n.d.	20.64	n.d.	0.03	0.04	0.31	6.66	6.64	91.02	11.28	0.00	4.82	0.00	0.01	0.00	0.07	2.56	1.69	1.11
MB-06–550-06	59.19	n.d.	23.34	n.d.	n.d.	0.07	0.15	7.65	7.04	97.44	11.03	0.00	5.13	0.00	0.00	0.00	0.03	2.77	1.68	1.14
MB-06–678-25	51.81	n.d.	24.79	0.01	0.03	0.06	0.54	6.01	7.27	90.52	10.02	0.00	5.62	0.00	0.01	0.00	0.15	2.82	1.94	1.14
MB-06–678-26	51.01	n.d.	24.45	0.01	0.08	0.33	0.47	6.46	7.94	90.75	10.22	0.00	5.75	0.00	0.03	0.01	0.13	3.17	2.25	1.03
MB-07–013-31	50.20	n.d.	27.46	n.d.	n.d.	0.16	0.13	7.80	7.80	93.55	10.07	0.00	6.04	0.00	0.00	0.02	0.02	2.83	2.49	1.13
MB-07–013-32	51.87	n.d.	26.59	0.03	n.d.	0.07	0.14	7.10	7.10	92.90	10.35	0.00	5.86	0.00	0.00	0.01	0.02	2.58	2.56	1.13

[a]n.d.: not detected.

The temperature calibration published in *Ghosh et al*. [2006] is used to determine mineral formation temperatures.

3.3.2. Oxygen and Hydrogen Isotopes on Silicates

Two whole-rock basalt clasts and 11 samples of chalcedony from individual vugs from a mineralized breccia specimen (MB-07-132) were analyzed for oxygen and hydrogen isotopes at the University of Oregon using CO_2-laser fluorination and TCEA integrated with MAT253 mass spectrometer [*Bindeman*, 2008; *Bindeman et al*., 2012]. For oxygen isotopes, ~1 mg single chunks cut by microsaw were loaded in a vacuum chamber together with standards and reacted in the presence of BrF_5 reagent to liberate oxygen gas. The gas generated in the laser chamber was purified through a series of cryogenic traps held at liquid nitrogen temperature, and a mercury diffusion pump was used to remove traces of fluorine gas. Oxygen was converted to CO_2 gas in a small platinum graphite converter, the yield was measured, and then CO_2 gas was analyzed on a MAT 253 mass spectrometer. Six garnet standards (UOG $\delta^{18}O$ 6.52‰) were analyzed together with the unknowns during analytical sessions. Samples were not pretreated overnight but rather a series of short pretreatments were performed. Sample yields ranged from 8 to 15 mol/mg suggesting that some opaline silica reacted with the reagent. However, no correlation of yield versus $\delta^{18}O$ value was observed, suggesting that the reaction was largely congruent, although it is possible that the OH portion of the opaline silica reacted preferentially explaining 0.4‰ lower $\delta^{18}O$ value of standards. Current investigation of $\delta^{18}O$ yield dependency on hydrous silicic glasses suggests maximum 0.4‰ upward shift with yield decreasing from 100 to 20% in this lab. Thus, the bias for minimal 50% yield of studied opaline silica standards was likely to

be less than 0.2‰. The measured $\delta^{18}O$ values of the standards were consistently 0.4‰ less than their empirical value, and unknown samples were adjusted to correct for this difference on the V-SMOW scale. The average precision on standards and duplicates of single grains and bulk analyses was better than 0.1‰.

For hydrogen isotope analysis of opaline silica, 5 mg single chunks that were cut adjacent to chunks used for O isotope analysis were crushed and sieved to size fractions less than 300 μm and greater than 50 μm, which is shown to be the best size range to extract water [*Bindeman et al*., 2012]. The samples, ranging from 3.6 to 5 mg, were loaded in silver cups, vacuum dried overnight at 150°C, and then immediately loaded into the He-purged carousel. The analyses were done using TCEA-MAT253 system by thermal pyrolysis into CO and H_2 gas using glassy carbon furnace held at 1450°C. We concurrently used three standards of mica spanning the D/H range of the unknown. The ^3H factor correction was performed in the morning and the data reduction included adding 25‰ to the value of the unknowns based on repeated measurement of the mica standard. Errors on water were better than 0.05 wt % and on δD better than 2.5‰ on single measurements.

3.3.3. Strontium Isotopes on Carbonates

Fifteen carbonate samples with Sr concentrations >1000 ppm (determined by EMP) were selected and analyzed in situ for $^{87}Sr/^{86}Sr$ ratios at the Woods Hole Oceanographic Institution. Analyses were performed using a New Wave 193 nm ArF Excimer laser ablation system coupled with a Thermo-Finnigan Neptune MC-ICPMS. Protocol, standard normalization and associated errors are described in *Jackson and Hart* [2006]. Line scans were performed on all 15 carbonate samples. Scans that produced a signal of less than 1 V on mass ^{88}Sr were not used as they created too large of systematic errors. Analyses of carbonates in five samples produced signal on mass ^{88}Sr greater than 1 V and they are reported in this study. Strontium values were corrected for Rb and Kr interferences. All data were normalized to the NBS 987 standard, $^{87}Sr/^{86}Sr = 0.71024$. Precision for analyses was ±0.0002 or better as compared to the standards ND-40-01 and NBS987.

4. Results

Hypocrystalline lava fragments and pyroclasts in all samples have a very similar primary (i.e., magmatic) mineral makeup. Phenocrysts in varying abundances consist of olivine, clinopyroxene, plagioclase, magnetite, and amphibole in vitric groundmasses that have been variably palagonitized. The mineral assemblage is characteristic of unaltered mafic compositions from other deposits at Minna Bluff [*Scanlan et al*., 2008; *Dunbar et al*., 2008; *Panter et al*., 2011]. Secondary minerals occur as intergranular cement and line open spaces within or surrounding clasts (Figure 3). Zeolites were initially identified in thin section based on morphology and later confirmed by XRD analyses. Zeolites that display a radial morphology are phillipsite and those with pseudocubic, rhombohedral forms are chabazite. Both zeolites are found in some samples ($n = 8$), other samples contain only phillipsite ($n = 19$) or only chabazite ($n = 9$). In a few samples zeolites show pronounced dissolution textures ($n = 4$) or are absent altogether ($n = 6$). Carbonates are present in all samples but varying in abundance and type, often showing very fine concentric zoning patterns (Figures 3a and 3d–3f) or as open-space fillings (Figure 3h). The most common carbonate textures are fibrous, prismatic, and microcrystalline types. Dogtooth-shaped carbonate crystal structures are also present in several samples (Figure 3e). Two other secondary minerals, dickite (a kaolin polymorph) and chalcedony, occur but are rare. In general, vug and vesicle fillings have a greater amount of chabazite and carbonates while fractures and interclast voids contain more phillipsite.

4.1. Mineral Paragenesis and Temperatures of Formation

The growth history of secondary minerals in altered volcaniclastic deposits at Minna Bluff is complex and includes occurrences of systematic as well as of nonsystematic variations in parageneses and chemistry. Phillipsite is most often found as the innermost mineral that line open spaces. Subsequent layers consist of either chabazite and/or carbonates (Figures 3b and 3h). Carbonates occur throughout the paragenetic sequence but most often form the final fill in open spaces with the exception of a few samples where the final filling mineral is chalcedony or dickite. For example, chalcedony forms the outer layer in vugs after magnesite in a mineralized breccia deposit (MB-07-132, Figure 3c) whereas dickite fills interclast voids after zeolite in a lapilli tuff (MB-07-172). Dickite is also found as the final fill in vesicles within lava clasts from another deposit of lapilli tuff (MB-06-656, Figure 3g).

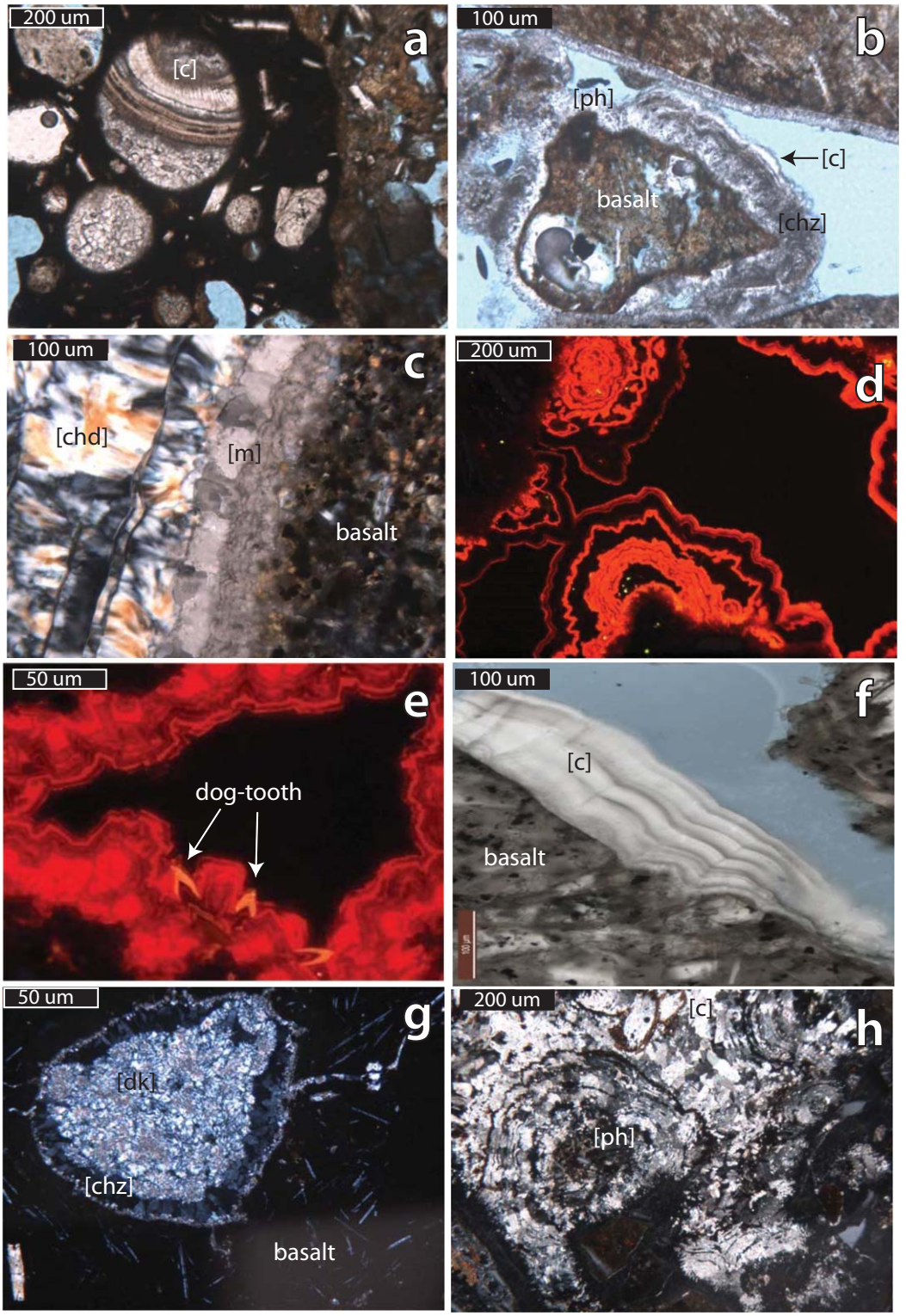

Figure 3. Photomicrographs showing representative images of alteration within volcanoclastic deposits at Minna Bluff. (a) Carbonates filling vesicles in clast from an altered lapilli tuff (sample MB-07-230). (b) Secondary minerals filling intergranular void within a polymict breccia (sample MB-06-801) in the order phillipsite (ph) → chabazite (chz) → carbonate (c). (c) Detail of a mineralized breccia (sample MB-07-132) with magnesite (m) before chalcedony (chd) filling a vein. (d) Cathode luminescence (CL) image that illustrates zoning in carbonate filling intergranular voids within a monomict breccia (sample MB-06-700). (e) CL image of "dog-tooth" carbonate crystals that terminate within a vug within mineralized breccia (sample MB-07-132). (f) Layering in carbonates that are filling intergranular void within a hyaloclastite breccia (sample MB-07-190). (g) Cross-polar image of vesicle lined by chabazite (chz) and filled by dickite (dk) in a clast from an agglutinate breccia (sample MB-06-656). (h) Phillipsite (ph) followed by carbonate (c) filling intergranular void within polymict hyaloclastite breccia (sample MB-06-775).

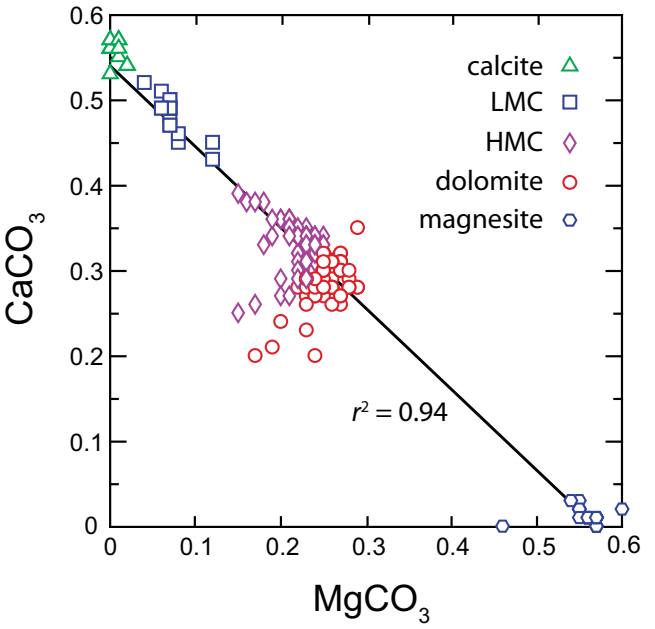

Figure 4. Plot of molar $MgCO_3$ versus $CaCO_3$ for carbonates measured in volcanoclastitic deposits at Minna Bluff. A linear regression of all carbonate analyses yields $r^2 = 0.94$. See text for the distinction between carbonate types based on mol %. Representative analyses of each of the five carbonate types are provided in Table 3.

In general, the assemblage of secondary minerals identified from Minna Bluff support low-temperature hydrothermal activity (≤200°C) characteristic of the palagonitization process [*Graham et al*., 2003; *Walton and Schiffman*, 2003]. Formation temperatures for alteration minerals like those found at Minna Bluff have been determined both experimentally and in natural systems. The temperature stability range for natural zeolites, phillipsite, and chabazite, formed by the hydrothermal alteration of Icelandic basalts is reported as >10 to ~100°C [*Kristmannsdottir and Tomasson*, 1978; *Apps*, 1983; *Jakobsson and Moore*, 1986] and experimentally up to 200°C [*Barth-Wirsching and Holler*, 1989]. Chabazite is stable at lower temperatures relative to phillipsite. *Jakobsson and Moore* [1986] document chabazite occurring at temperatures <50–92°C and phillipsite at 55–105°C in altered basalts from the Surtsey volcano, Iceland. Carbonates can form in volcanic geothermal systems over a very broad range of temperatures (up to 270°C) [*Apps*, 1983] and can be one of the first alteration minerals to crystallize [e.g., *Jakobsson and Moore*, 1986], or can be contemporaneous with phillipsite [e.g., *Konya and Szakall*, 2011], or paragenetically later than all zeolite-group minerals [e.g., *Konya and Szakall*, 2011]. All three types of paragenetic associations were observed in this study. Magnesite is reported to be the most stable carbonate phase at higher temperatures [*Boschi et al*., 2009]. The temperature stability range of chalcedony in hydrothermally altered basalts is reported as ~10–150°C [*Apps*, 1983; *Jakobsson and Moore*, 1986; *Morteani et al*., 2010; *Gysi and Stefánsson*, 2012], and the clay mineral dickite is reported to be transformed from kaolinite when temperatures are greater than 120°C [*Reyes*, 1990; *Ehrenberg et al*., 1993].

4.2. Chemistry and Zoning in Zeolites and Carbonates

Representative chemical analyses of phillipsite $(Ca_{0.5}, K, Na)_6 [Al_6Si_{10}O_{32}]\cdot 12H_2O$ and chabazite $(Ca, K_2, Na_2)_2 [Al_4Si_8O_{24}]\cdot 12H_2O$ are presented in Table 2. These alkali zeolites are classified following *Coombs et al*. [1997] as chabazite-K(Na) and phillipsite-K(Na). The ratio of (Na + K)/Ca is highly variable for phillipsite (range 0.9–181.0 and mean = 56.1 ± 42.4) and chabazite (range 8.7–97.0 and mean = 28.8 ± 21.0) between deposits as

Table 3. Major Element Abundances of Representative Carbonates From Minna Bluff[a]

		Weight Percent Oxides					$MgCO_3$
Carbonate Type	Sample	CaO	MgO	MnO	FeO	SrO	mol %
Calcite	MB-07-148-2182	54.56	0.60	0.01	0.01	n.d.	1.30
LMC[b]	MB-06-560-12	49.04	6.13	n.d.	n.d.	n.d.	12.92
HMC[c]	MB-07-013-2	35.83	17.79	0.10	0.12	n.d.	37.09
Dolomite	MB-07-118-238	27.66	23.81	n.d.	0.19	n.d.	50.54
Magnesite	MB-07-132-10	0.83	47.69	n.d.	n.d.	n.d.	98.55
Siderite	MB-07-190-2132	14.19	13.85	0.09	14.12	0.20	53.68

[a]n.d.: not detected.
[b]Low magnesium carbonate.
[c]High magnesium carbonate.

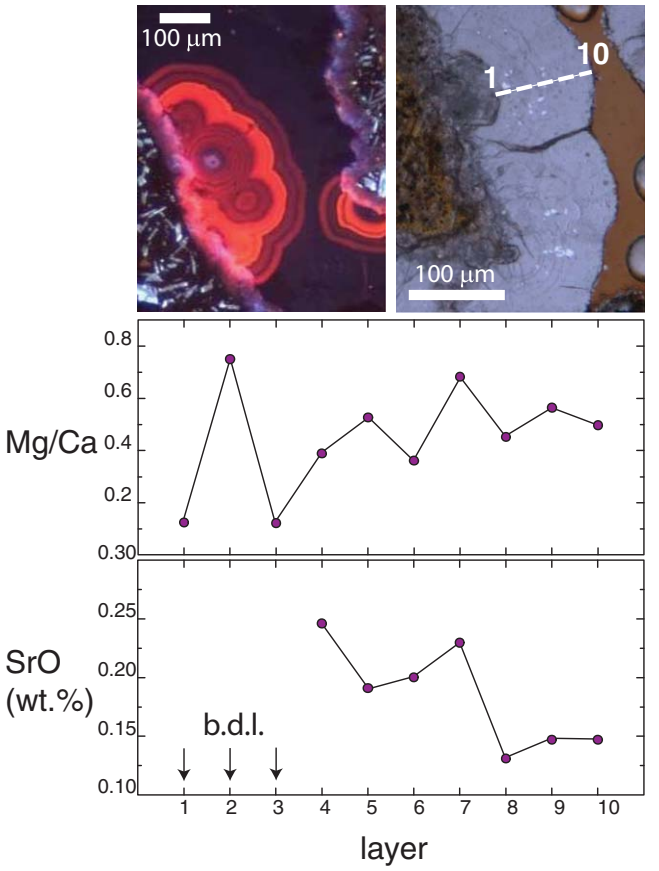

Figure 5. Variations in SrO (wt %) and Mg/Ca ratios across layers in carbonate from sample MB-06-560. Strontium concentration is below detection limit (b.d.l. < 1000 ppm) in layers 1 to 3. The approximate location of the microprobe traverse is shown by the dotted line in the image taken in plane polarized light. The cathode luminescence image shows the compositional complexity of carbonate layering within the same sample (MB-06-560).

well as oftentimes between open-space types and layers within an individual sample. Despite their similarity in composition (Figure 7), chabazite is statistically distinct from phillipsite ($p < 10^{-3}$) based on Hotelling's T^2 test [*Hammer and Harper*, 2006]. Compositional differences between layers in chabazite are also significant ($p < 10^{-5}$), but for phillipsite the layers are chemically homogeneous ($p > 0.4$).

Carbonate minerals occur in all 24 samples analyzed. All analyses ($n = 251$) are shown in Figure 4, and representative analyses for each carbonate phase are shown in Table 3. Carbonates consist of calcite with <3% $MgCO_3$ [mol % = ($MgCO_3$/($MgCO_3 + CaCO_3$))*100], low Mg-calcite (LMC) defined as having ≥3 to <22% $MgCO_3$, high Mg-calcite (HMC) with ≥22 to <44% $MgCO_3$, dolomite (≥44 to <55% $MgCO_3$), and magnesite (>94% $MgCO_3$). Several carbonate analyses approach end-member siderite ($FeCO_3$) and rhodochrosite ($MnCO_3$) compositions. The covariance of $MgCO_3$ with $CaCO_3$ in carbonates (Figure 4) is significant with 95% of the analyses ($r^2 = 0.94$). A few HMC and dolomite analyses fall significantly below the line of regression indicating substitution of other cations (e.g., Fe, Mn, and Sr) for Mg in the carbonate lattice.

Layering in carbonates often show significant compositional variations. Chemical profiles indicate progressive chemical changes from inner to outer layers, while others show nonsystematic variations. For example, carbonate precipitated within interclast voids in sample MB-06-560 shows significant chemical variations and an overall increase in Mg/Ca ratios and decrease in Sr concentration between the innermost and outermost layers (Figure 5). Other chemical transects (not shown) have relatively uniform compositions across layers such as in sample MB-06-523 where Mg/Ca ratios vary from 0.69 to 0.74 [*Antibus*, 2012]. The fine concentric zoning patterns revealed under cathode luminescence are seldom truncated by re-growth. This, along with the fact that euhedral, terminated, carbonate structures are often the final filling in open spaces (Figures 3–3f and 5), strongly suggests that dissolution and reprecipitation by fluids unrelated to the primary phase of alteration was rare.

4.3. Isotopic Signatures of Secondary Minerals

Oxygen and carbon isotopes were measured on carbonates in 13 samples (Table 4). Oxygen and carbon isotopic values positively correlate and have a wide range of values ($\delta^{18}O_{V\text{-}SMOW} = -0.50$ to 21.53‰ and $\delta^{13}C_{V\text{-}PDB} = -1.04$ to 8.98‰). Carbonates show progressively higher $\delta^{18}O$ values with increasing Mg content and, statistically, carbonates with higher Mg contents (i.e., dolomite, HMC, and magnesite) have $\delta^{18}O$ and $\delta^{13}C$ values that are distinguishable from low Mg carbonates and calcite ($p = 0.02$). This positive correlation between $\delta^{18}O$ and Mg content in carbonates has been recognized elsewhere [e.g., *Kralik et al.*, 1989; *Best*

Table 4. Isotope Analyses (O, C, H, Sr) for Carbonates, Chalcedony, and Basalt From Minna Bluff[a]

Sample	Mineral	Void Type	Method	$\delta^{18}O_{VSMOW}$	$\delta^{13}C_{VPDB}$	δD_{VSMOW}	$^{87}Sr/^{86}Sr$	Δ_{47} (°C)	$\delta^{18}O_{water}$
MB-07-013	HMC	Vein	MM	9.54	5.25				
MB-07-013	HMC	Vug	MM	7.74	5.16				
MB-07-102	HMC	Vug	Conv	13.67	3.60				
MB-07-111	Dolomite	Intergranular	Conv	18.58	4.77				
MB-07-118	HMC	Vesicle	LA				0.702981		
MB-07-118	HMC	Vesicle	Conv	17.59	6.05				
MB-07-118	HMC	Vesicle	Clump	16.36	5.83			5.0	−19.9
MB-07-132	Magnesite	Vug (i)	MM	6.11	4.08				
MB-07-132	Magnesite	Vug (o)	MM	3.81	−1.04				
MB-07-132	Chalcedony	Vug (f)	O-H	4.28		−206.4			
MB-07-132	Chalcedony	Vug (i)	O-H	7.83		−205.7			
MB-07-132	Chalcedony	Vein	O-H	1.65		−194.9			
MB-07-132	Chalcedony	Vug (o)	O-H	5.37		−210.4			
MB-07-132	Basalt	Clast		3.25					
MB-07-148	Dolomite	Vug (o)	MM	8.28	−1.04				
MB-07-190	HMC	Intergranular	Conv	19.49	7.73				
MB-06-515	Dolomite	Intergranular	Conv	8.50	3.91				
MB-06-523	Dolomite	Intergranular	LA				0.703635		
MB-06-523	Dolomite	Intergranular	Conv	14.91	4.86				
MB-06-529	Dolomite	Intergranular	LA				0.704752		
MB-06-550	Dolomite	Vug (i)	LA				0.703319		
MB-06-550	Dolomite	Vug (i)	LA				0.702402		
MB-06-550	Dolomite	Vug	Conv	7.29	3.01				
MB-06-554	Calcite	Vein	Conv	4.22	1.08				
MB-06-554	Calcite	Intergranular	MM	−0.50	1.73				
MB-06-554	Calcite	Intergranular	Clump	1.52	1.38			42.7	−22.9
MB-06-560	HMC	Vug	LA				0.702712		
MB-06-560	HMC	Vug	Conv	12.58	5.54				
MB-06-560	HMC	Vein	MM	11.96	5.54				
MB-06-560	HMC	Vug	Clump	10.65	5.53			20.5	−21.4
MB-06-567	Magnesite	Vein	Conv	15.03	5.56				
MB-06-567	Magnesite	Vug	Conv	14.04	5.26				
MB-06-567	Magnesite	Vug (o)	MM	16.02	5.37				
MB-06-623	Dolomite	Vesicle	Conv	16.69	8.98				
MB-06-623	Dolomite	Vesicle	Clump	16.59	8.89			20.0	−15.8
MB-06-626	Magnesite	Vug (o)	MM	18.24	6.60				
MB-06-656	Dolomite	Vesicle	Conv	21.53	5.23				
MB-06-678	LMC	Vug	Conv	5.58	1.81				
MB-06-700	Dolomite	Vug (i)	MM	14.11	2.15				
MB-06-700	Dolomite	Vug (o)	MM	13.55	3.12				
MB-06-724	Dolomite	Intergranular	Clump	12.32	3.19			10.2	−22.4

[a]Notes: stable isotope values (O, C, D) measured in per mil (‰); water temperatures for clumped isotope data were determined from analyses according to *Ghosh et al.* [2006] as recalculated by *Dennis et al.* [2011]. Oxygen isotope values for water in equilibrium with carbonates calculated based on ^{13}C-^{18}O thermometry (see text for details). Abbreviations: low magnesium carbonates (LMC); high magnesium carbonate (HMC); conventional sampling for C-O isotopes (Conv); micromill sampling for C-O (MM); clumped analysis of C-O (Clump); oxygen-hydrogen isotope analysis (O-H); strontium isotopes sampled by in situ laser ablation (LA); outer rim (o); inner rim (i); filling mineral (f).

et al., 2000; *Herrero et al.*, 2011] but of special note is the exceptionally wide range of $\delta^{18}O$ values ($\Delta > 21‰$) at Minna Bluff (Table 4). Documented cases for comparison include $\delta^{18}O$ values of hydrothermally altered platform carbonates from northwestern Spain that vary by $\sim 10‰$ [*Shah et al.*, 2012]. Also, carbonates found within hydrothermally altered lavas from the Kerguelen Archipelago [*Renac et al.*, 2010] have nearly as wide a range but are slightly heavier ($\delta^{18}O = 8.7$ to $27.4‰$) and have much lighter $\delta^{13}C$ values (-11.69 to $0.68‰$), relative to the carbonates from Minna Bluff.

Samples of carbonates obtained by the micromilling of individual layers reveal small-scale isotopic heterogeneities. Inner and outer layers of carbonates within vugs were measured in two samples and the results are shown in Figure 6. The inner layer of magnesite in mineralized breccia sample MB-07-132 has a higher $\delta^{18}O$ ($6.11‰$) than the outer layer ($3.81‰$). In contrast, the inner layer of dolomite from a vug in sample MB-06-700 has only a slightly heavier $\delta^{18}O$ value but a noticeably lower $\delta^{13}C$ value than the outer layer of dolomite (Figure 6). Differences in oxygen isotopes were also noted between carbonate layers within the same sample but from different areas and open-space types (e.g., MB-07-013 and MB-06-567; Figure 6).

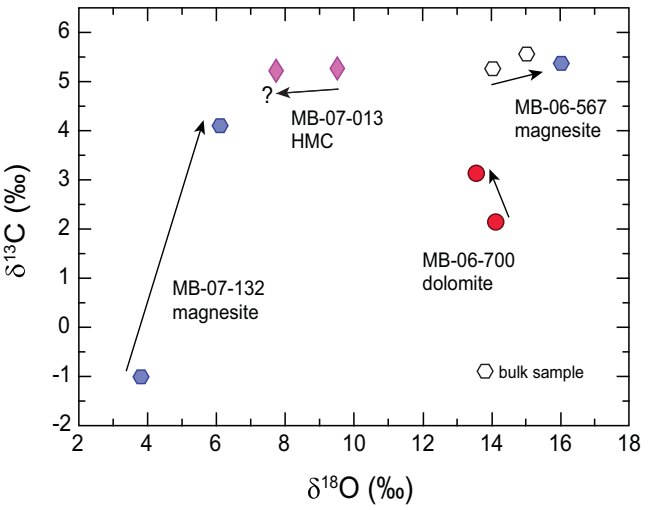

Figure 6. Plot of $\delta^{18}O$ versus $\delta^{13}C$ for magnesium-rich carbonates. Results from sampling by micromilling (filled symbols) show that the chemical zoning, originally identified through petrography and cathode luminescence (Figures 3 and 5), is also expressed by complex variations in stable isotope values. Bulk sample analyses (open hexagons) for MB-06-567 represent carbonates collected from two different void types (Table 4). Arrows indicate carbonate parageneses (i.e., inner → outer layers) for minerals filling vugs and veins. Errors (±0.1‰) are contained within the size of each symbol.

Isotopes of oxygen were measured on chalcedony from a mineralized breccia (MB-07-132). The $\delta^{18}O$ values of chalcedony collected from individual vugs have a broad range from 0.68 to 10.37‰ [*Antibus*, 2012; *Bindeman et al*., 2014], one sample collected from a filled fracture yields a value of 1.7‰, and two analyses of whole-rock clasts, representative of altered basalt, yield values of 3.0 and 3.5‰ (Table 4). Visible zoning in the chalcedony allowed for the separation and analysis of cores (i.e., layers closest to the host rock) and rims (i.e., outermost layers) in several places. The $\delta^{18}O$ of cores overlap but have an overall lower range (0.68–7.4‰, $n = 6$) relative to the rims (5.4–10.37‰, $n = 5$). Statistically, differences in $\delta^{18}O$ between individual core-rim pairs were not found to be significant ($p > 0.24$). This sample yields extremely light hydrogen isotopes with δD values that range from −187.8 to −210.4‰ (Table 4).

Isotopes of strontium measured on carbonates from five different samples yield similar values (Table 4). The average $^{87}Sr/^{86}Sr$ ratios for three samples measured multiple times are 0.702861 (±0.000648, 1σ, $n = 2$), 0.703563 (±0.00036, 1σ, $n = 5$), and 0.704299 (±0.002092, 1σ, $n = 3$). Single spot analyses from two other samples yield values of 0.702981 and 0.702712 (both with analytical uncertainty of ±0.0002, or better, at 1σ). The samples represent deposits that range in elevation from 50 to 624 m above sea level (m asl) and range between 8.79 and >11.44 Ma based on $^{40}Ar/^{39}Ar$ ages determined directly from the deposit ($n = 4$) or from lava overlying the deposit (MB-06–550; Tables 1 and 4).

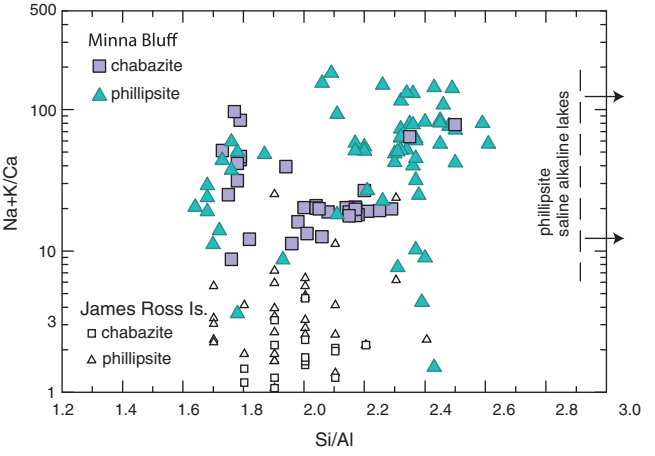

Figure 7. Plot of Si/Al versus (Na + K)/Ca ratios for phillipsite and chabazite from Minna Bluff (Table 2) and James Ross Island, Antarctica [*Johnson and Smellie*, 2007]. Also shown for comparison is the lower range in Si/Al ratios determined for phillipsite formed by the alteration of volcanic glass in saline alkaline lake environments [*Sheppard and Fitzpatrick*, 1989; *Surdam and Eugster*, 1976].

5. Discussion

5.1. Water Source for Alteration

One of the main objectives of this study is to determine the conditions and type of water (i.e., seawater versus freshwater) involved in the formation and alteration of primary glass-rich volcaniclastic deposits at Minna Bluff with the purpose being to reconstruct the original eruptive environments. Chemical and isotopic properties of secondary minerals in volcaniclastic deposits, in particular palagonitized hyaloclastites, have been used by others to investigate alteration

processes and water types [*Walton and Schiffman*, 2003; *Johnson and Smellie*, 2007; *Marks et al*., 2010]. Magnesium-rich carbonates (e.g., dolomite and magnesite) can precipitate from seawater [*Major and Wilber*, 1991; *Carpenter et al*., 1991], saline lake water [*Larsen*, 2008; *Flügel*, 2010] as well as in hydrothermal environments not associated with volcanic systems [*Shah et al*., 2012]. However, the composition of carbonates in Minna Bluff volcaniclastic deposits are similar to carbonates reported from volcanic activity-induced hydrothermal systems [*Jakobsson and Moore*, 1986; *Renac et al*., 2010] and, morphologically, often show dogtooth-shaped crystal forms (Figure 3e) that are indicative of volcanic-related hot spring type environments [*Flügel*, 2010]. Fluids with elevated CO_2 contents can mobilize Ca, Mg, and Fe, and at lower temperatures, these fluids can precipitate Ca-Mg-Fe carbonates [*Destrigneville et al*., 1991; *Gysi and Stefánsson*, 2012]. The formation of Mg-rich carbonates at Minna Bluff is a likely consequence of high magmatic CO_2 contents in the alteration fluids. This is a reasonable hypothesis given the levels of CO_2 measured in melt inclusions from other alkaline volcanic rocks (basanite to phonolite) in the Erebus Volcanic Province as well as the high CO_2 emission rates measured at the currently active Mount Erebus volcano [*Wardell et al*., 2004; *Oppenheimer et al*., 2011].

The water source type from which carbonates precipitated can be constrained by oxygen isotopes but only if formation temperatures are known. Five carbonate samples from Minna Bluff contain sufficient carbonate material to measure $\delta^{13}C$ and $\delta^{18}O$ for "clumped isotope" thermometry [*Eiler*, 2007]. Formation temperatures determined from ^{13}C-^{18}O relationships [*Ghosh et al*., 2006] range from $\Delta_{47} = 5.0$ to 42.7°C with a median value of 20°C (Table 4). These temperature values for carbonates fall within the lower range of temperatures estimated for zeolite stability in modern geothermal systems (>10 to ~100°C) [*Kristmannsdottir and Tomasson*, 1978; *Apps*, 1983; *Jakobsson and Moore*, 1986]. However, considering the fact that zeolites in most of the deposits are often the first open-space filling mineral followed by carbonates, then it is likely that the carbonates formed at lower temperatures relative to zeolites in a cooling hydrothermal system. Using temperatures from ^{13}C-^{18}O thermometry and composition-appropriate fractionation factors [*O'Neil et al*., 1969; *Böttcher*, 1994; *Sharma et al*., 2002], the calculated $\delta^{18}O$ of water in equilibrium with Minna Bluff carbonates range from −15.8 to −22.9‰ (Table 4). The ^{18}O-depleted water values determined for the five carbonate samples along with the light deuterium values measured on opaline silica (−187.8 to −210.4‰; Table 4) indicate that the parent fluids for carbonates and the fluids that hydrated silica were derived from Antarctic freshwater sources, as opposed to seawater. While oxygen and deuterium isotopic values determined for water are light, their range is not as light as modern ice and snow in McMurdo Sound ($\delta^{18}O = -25$ to −35‰, $\delta D = -200$ to −280‰) [*Stewart*, 1975; *Kellogg et al*., 1991; *Fitzsimons et al*., 2012]. This difference and the implication for the reconstruction of past climate in this region will be discussed below.

Strontium isotopes also provide a highly sensitive indicator of water type [*Dennison et al*., 1998; *Barbieri and Morotti*, 2003; *Marcano et al*., 2009]. Unlike oxygen isotopes, the incorporation of Sr into carbonate structures is not temperature dependent. The $^{87}Sr/^{86}Sr$ ratio of seawater is well known through the Cenozoic, and the $^{87}Sr/^{86}Sr$ ratio in freshwater will reflect the isotopic composition of the rocks being altered [*Fisher and Stueber*, 1976]. Thus, the water source can be determined directly by measuring the carbonate $^{87}Sr/^{86}Sr$ ratio [*Tucker and Wright*, 1990]. Middle Miocene to modern seawater values range from 0.7086 to 0.7092 [*Faure and Mensing*, 2005] and alkaline volcanic rocks in the Erebus Volcanic Province, which are similar in major and trace element composition to those at Minna Bluff, have whole-rock values that range from 0.7029 to 0.7050 [*Kyle*, 1990; *Kyle et al*., 1992; *Panter et al*., 2003; *Sims et al*., 2008; *Rilling*, 2009; *Martin et al*., 2013]. The $^{87}Sr/^{86}Sr$ values measured in this study (0.7027–0.7043; Table 4) are in the range expected for carbonates precipitated by fresh meteoric waters that has exchanged only with local volcanic rocks. It should be noted, however, that for rock-dominated systems (i.e., low water to rock ratios) the Sr isotopic composition of the volcanic deposits may obscure the original signature of the interacting fluid. Nonetheless, these results, together with the highly depleted oxygen values calculated for carbonates, favor an original freshwater source for the alteration fluids.

Zeolites mostly formed before carbonates during the alteration of volcanoclastic deposits at Minna Bluff. *Johnson and Smellie* [2007] use (Na + K)/Ca ratios measured on phillipsite and chabazite to distinguish seawater from freshwater alteration of hyaloclastite deposits at James Ross Island, Antarctica. They employed previously published zeolite compositions from known terrestrial and marine environments to delimit the two water sources. They conclude that alteration by seawater produced phillipsite and chabazite with

(Na + K)/Ca ratios greater than 3.0 and 1.0, respectively, and alteration by freshwater produced zeolites with alkali ratios below those values. The application of this chemical proxy for the water type responsible for the formation of zeolites at Minna Bluff would suggest that all chabazite and nearly all phillipsite were formed from seawater (Figure 7). But we consider this to be highly unlikely given, in part, to the fact that zeolites with high (Na + K)/Ca ratios occur at all elevations, including deposits that lie well over 700 m asl.

In summary, the physical, chemical, and isotopic evidence indicates that the alteration of volcaniclastic deposits at Minna Bluff is the result of interactions between meteoric water (e.g., melted snow and ice) and highly reactive volcanic glass. Therefore, we can assume that the geochemical and isotopic variability of carbonates and zeolites is primarily the result of changing physiochemical conditions during their formation (e.g., temperature, pH, total dissolved solids) and not related to changes in water source type.

5.2. Alteration Environment

A simple, coherent, synthesis of the alteration history of volcaniclastic deposits at Minna Bluff is not possible. This is because the alteration of each deposit is considered to have occurred as an isolated, short-term hydrothermal episode with heat and water supplied either directly during the quenching and granulation of magmas (i.e., hyaloclastites) or by newly erupted volcanic material emplaced in close proximity to wet sediments. This premise is supported by field observations that record the sporadic and spatially restricted occurrences of these deposits [*Wilch et al*., 2011] (Figure 1) as well as the absence of extensive zones of alteration and lack of mineralized halos along faults that cut through the well-exposed stratigraphy at Minna Hook. Additionally, the poor correlation ($r^2 < 0.4$) of geochemical indices for alteration with stratigraphy, elevation, and age [*Antibus*, 2012] also suggests that the alteration occurred as isolated events. Furthermore, the occurrence of phillipsite as a single chemically homogeneous layer, often forming the innermost lining in cavities, supports its growth during the earliest stage of alteration; i.e., not a product of a later or unrelated phase of alteration. Weathering is also not considered to be a significant factor based on the dearth of carbonate dissolution features (as discussed above). Finally, the high formation temperatures estimated for zeolites, Mg-rich carbonates, and chalcedony, and the polar to subpolar conditions that have existed since their formation, all indicate that they are *primary* alteration phases.

Small-scale circulation implies a more limited water supply and hydrothermal systems that are rock-dominated. A simple, quantitative estimate of the proportion of water to rock is calculated for mineralized breccia (sample MB-07-132; Figures 2c and 2d) using the measured $\delta^{18}O$ of altered basalt (3.1 and 3.5‰, Table 4) an estimate of unaltered basalt (5.5–6.0‰), modern water values for McMurdo Sound (−25 to −35‰), and *Taylor's* [1977] equations for isotopic equilibration between rock and water in both open and closed hydrothermal systems. The models predict low water to rock ratios ($w/r < 1$) for temperatures of exchange between 25 and 100°C. Higher temperatures of alteration (>90°C), and consequently very low water to rock ratios ($w/r \sim 0.15$), are estimated using the quartz-calcite thermometer of *Sharp and Krischner* [1994] and, empirically, by the absence of chabazite and phillipsite, and presence of magnesite. Temperatures much over 100°C exceed the stability limits of these zeolites and can explain their absence in this sample (MB-07-132) as well as in other deposits. Following this thread of reasoning, fluid boiling or high rates of evaporation at or near the surface would lead to the loss of CO_2 and increase the pH thus promoting Mg-carbonate precipitation which, in turn, increases silica activity and precipitation of chalcedony after magnesite (e.g., Figure 3c). Higher temperatures of alteration are also implied for two other deposits (MB-06-656 and MB-07-172) based on the occurrence of the clay mineral dickite, which replaces kaolinite at temperatures in excess of 100°C [*Reyes*, 1990; *Ehrenberg et al*., 1993].

The alteration of volcaniclastic deposits by hydrothermal meteoric water at low water to rock ratios will produce zeolites with high (Na + K)/Ca ratios (Figure 7). Phillipsite and chabazite compositions with high (Na + K)/Ca ratios have been reported in basaltic lavas that have been hydrothermally altered by seawater [e.g., *Böhlke et al*., 1980; *Johnson and Smellie*, 2007, and references therein] and in vitric tuffs altered by saline, alkaline lake waters at lower temperatures [e.g., *Hay*, 1978; *Surdam and Sheppard*, 1978; *Larsen*, 2008]. The (Na + K)/Ca composition of chabazite and phillipsite from Minna Bluff have very similar (Na + K)/Ca ratios to those precipitated from lake water associated with closed hydrological systems [*Hay*, 1964; *Surdam and Eugster*, 1976; *Sheppard and Fitzpatrick*, 1989] but with much lower Si/Al ratios (Figure 7). In contrast, zeolites that are formed in open hydrological systems tend to favor calcium-rich zeolite species [*Ibrahim*, 2004] which do not occur at Minna Bluff. In lake environments zeolites can form in relatively short periods

of time (e.g., 1000 years) [*Hay*, 1964, 1966] and in the case of volcanic-induced hydrothermal conditions may take as little as 6 months to just a few years [*Jakobsson and Moore*, 1986; *Jakobsson and Guomundsson*, 2012]. This reaffirms our earlier conclusion that the alteration at Minna Bluff occurred during, or very soon after, the formation of each deposit.

Volcaniclastic facies formed by local interactions between volcanic activity and surficial water sources or glaciers involves the complex interplay of eruptive, depositional, and hydrological processes [*Smellie*, 2000], all of which promote a dynamic environment for alteration. The hydrothermal alteration of tephra and volcaniclastic sediments at Minna Bluff occurred under variable conditions with respect to temperature and fluid chemistry. This is evident in the broad compositional range of carbonates and zeolites (Figures 5–7) and their diverse textures (Figure 3). Complex chemical zoning in carbonates revealed by cathode luminescence (Figures 3d, 3e, and 5) suggests that these small, closed hydrologic systems may have fluctuated between oxic and more anoxic conditions [*Carpenter and Oglesby*, 1976; *Barnaby and Rimstadt*, 1986; *Horbury and Adams*, 1989]. *Larsen* [2008] interpreted differences in the chemistry and the paragenesis of secondary minerals found in altered tuff within a saline lake to be the result of episodic influx of freshwater. At Minna Bluff we envisage rapid and dynamic changes in the physical and chemical conditions during alteration that would be expected for episodic volcanic activity in terrestrial environments where water is readily available but finite (e.g., melting of thin, local ice caps or snowfields). Although it is difficult to constrain the specific cause of the variations in secondary minerals at Minna Bluff, rapid changes in fluid chemistry in response to temperature fluctuations and sudden input/release of magmatic gases (e.g., CO_2) are expected in a rock-dominated, small-scale, eruption-induced, hydrothermal system.

5.3. Implications for Paleoclimate

If secondary minerals were precipitated from the same meteoric waters that were involved in the original formation and deposition of the glass-rich volcaniclastic materials, and the oxygen isotopic composition of that water can be determined, then variations in the $\delta^{18}O$ of the water may provide information on past Antarctic climates, as δD has recently been used [*Feakins et al*., 2012]. We propose that carbonates in volcaniclastic deposits at Minna Bluff can provide a proxy for paleoclimate that is independent of other climate records from this region.

Since it is critical to know the temperature at which the minerals formed to determine the oxygen isotope composition of the waters that precipitated them, we compare the measured $\delta^{18}O$ of minerals that have temperatures of exchange estimated by ^{13}C-^{18}O [*Ghosh et al*., 2006] and quartz-calcite [*Sharp and Krischner*, 1994] thermometry with $\delta^{18}O$ of minerals modeled over a range of possible formation temperatures (Figure 8). The model $\delta^{18}O_{mineral}$ curves in Figure 8 were derived using model $\delta^{18}O$ water values calculated over a range of mean annual atmospheric temperatures estimated for the Late Miocene in the McMurdo Sound area [*McKay et al*., 2009]. *McKay et al*. [2009] based these estimates on stratigraphic sequences recovered from the AND-1B drill core, which is located $<$100 km to the north of Minna Bluff (Figure 1). Three glacial regimes reconstructed from modern environments are used to predict mean annual atmospheric temperatures associated with the deposition of sedimentary sequence packages (a.k.a. *Motifs*). Air temperature variations during the time of Minna Bluff's formation ($\sim$12 to $\sim$4 Ma) are reconstructed based on three of these sedimentary motifs of *McKay et al*. [2009] and chronostratigraphic data from *Wilson et al*. [2012]. Motif 1 is similar to the modern polar climate regime of McMurdo Sound with a mean annual air temperature of $-17^{\circ}C$ for the time period from $\sim$12.5 to 9.5 Ma. Motif 3 indicates a warmer, subpolar environment with an annual mean air temperature $-6.4^{\circ}C$ over a period from $\sim$9.5 to $\sim$8.0 Ma. Motif 2b represents a cooler, subpolar climate between $\sim$5 and $\sim$3 Ma with a mean annual air temperature of $-7.6^{\circ}C$. The $\delta^{18}O$ of water precipitated in Antarctica over this range of air temperatures can vary by as much as 8.5‰ [*Masson-Delmotte et al*., 2008].

The measured $\delta^{18}O$ of dolomite/HMC, calcite/LMC, and chalcedony samples, which have estimated temperatures of formation, are in good agreement with model values calculated using meteoric water precipitated over a range of possible air temperatures (Figures 8a–8c). The measured magnesite, however, is significantly heavier than the model $\delta^{18}O$ values (Figure 8d). The relatively heavy $\delta^{18}O$ of magnesite (sample MB-07–132) may be explained by ^{18}O-enrichment from evaporative distillation [*Kralik et al*., 1989; *Schroll*, 2002]. The $\delta^{18}O$ of water calculated for chalcedony and the δD measured on opaline silica from the same sample (MB-07–132) plot to the right of the local meteoric water line (Figure 9). While it is possible that the shift away

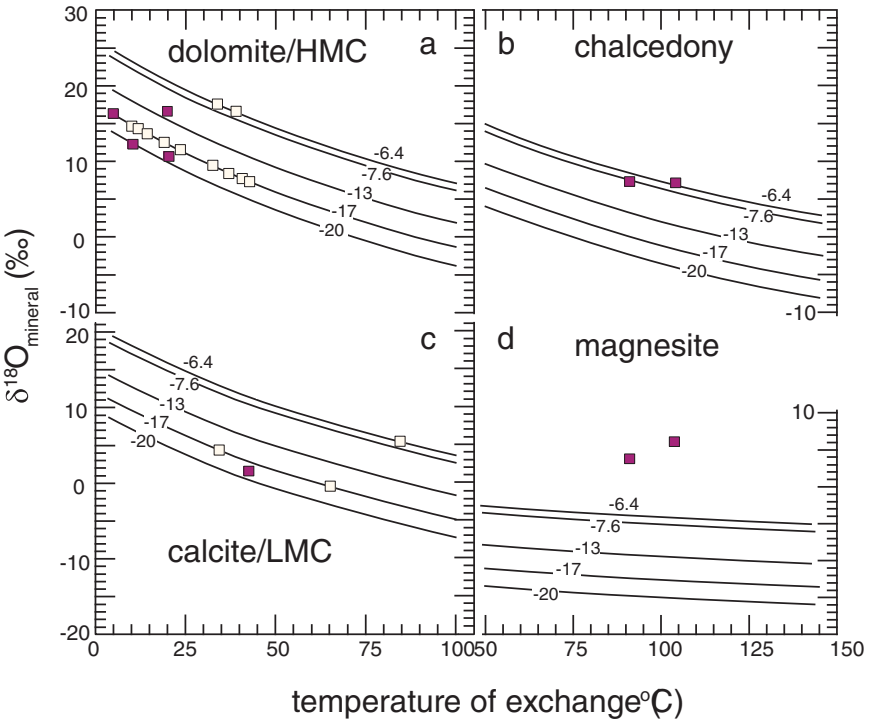

Figure 8. Plots of temperature of exchange ($^{18}O/^{16}O_{mineral} \leftrightarrow {}^{18}O/^{16}O_{water}$) versus mineral $\delta^{18}O$. Maroon squares signify formation temperatures determined by ^{13}O-^{18}O thermometry [cf., *Gosh et al*., 2006] for (a) dolomite/HMC and (c) calcite/LMC or quartz-calcite thermometry [*Sharp and Kirschner*, 1994] for (b) chalcedony and (d) coexisting magnesite. Curves represent model $\delta^{18}O$ values for minerals determined using meteoric water values calculated based on the relationship between air temperature and Antarctic snow [*Masson-Delmotte et al*., 2008] along with mineral and temperature-appropriate fractionation factors [*Friedman and O'Neil*, 1977; *Kawabe*, 1979; *Sharma et al*., 2002]. Note that the two samples of magnesite (Figure 8d) plot above model curves at any temperature of exchange (see text for details). Carbonate samples without thermometry (open squares) are plotted where the measured $\delta^{18}O$ value for each sample intersects the $\delta^{18}O_{mineral}$ model curve that matches the mean annual air temperature predicted for the region [*McKay et al*., 2009] at the time the deposit was formed (Table 1).

from the meteoric water line to heavier $\delta^{18}O_{water}$ values may be caused by mixing between different, variably exchanged waters [e.g., *Blattner*, 1985; *Scott*, 2004], it is more likely a consequence of steam loss from hot spring geothermal waters generated by volcanic activity.

Calculated $\delta^{18}O_{water}$ for calcite/LMC and dolomite/HMC are plotted against age and compared to glacial regimes derived from the AND-1B and AND-2A drillcores in Figure 10. While the age of the volcaniclastic deposits from Minna Bluff are reasonably well constrained (Table 1), the age of the drillcores are not as well constrained over the same time interval [*Acton et al*., 2008; *Di Vincenzo et al*., 2009; *Wilson et al*., 2012], and therefore the age comparison is tenuous. Nevertheless, it is intriguing to note that there is a broad shift from lighter to heavier water values that corresponds with the change from colder to warmer glacial regimes (Motif 1 $\rightarrow$ 3) as predicted by *McKay et al*. [2009]. Cold conditions prior to 9 Ma also is supported by $\delta^{18}O$ and δD results from chalcedony (sample MB-07–132, $>$9.42 Ma, Table 1). This interpretation is made by simply subtracting the projected ^{18}O-enrichment back to the meteoric water line in Figure 9 which yields an initial $\delta^{18}O_{water}$ around $-25‰$. The intersection with the meteoric water line coincides with the heavier end of the range for modern meteoric waters from the McMurdo Ice Shelf [*Kellogg et al*., 1991; *Fitzsimons et al*., 2012] and is indicative of polar conditions for that time.

Smellie et al. [2014] use the same glaciovolcanic sequences, which include the hyaloclastite deposits in this study, to reconstruct paleoice conditions at Minna Bluff and for other Neogene ($<$12 Ma) glaciovolcanic sequences in Victoria Land. Their results indicate polythermal regimes that range from wet-based to cold-based ice conditions in different regions at roughly the same time. This is in contrast with other studies that call upon a step-wise transition to cold-based conditions everywhere sometime after the middle Miocene [e.g., *Lewis et al*., 2007]. Specifically, *Smellie et al*. [2014] conclude that over the period 11.5–9 Ma the basal ice conditions at Minna Bluff were warmer ("thawed based") than at the AND-1B and AND-2A drillsites. Their

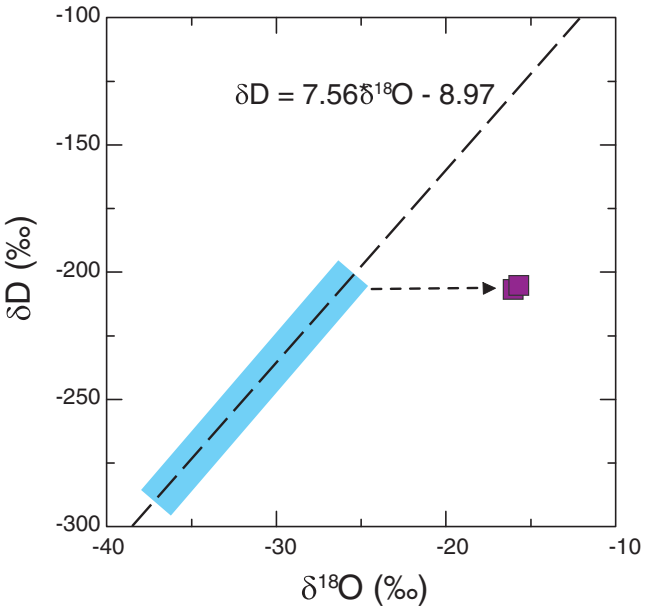

Figure 9. Relationship between $\delta^{18}O$ and δD of meteoric water in McMurdo Sound. Chalcedony and opaline silica from sample MB-07-132 plot to the right of the meteoric water line of *Fitzsimons et al.* [2012]. The displacement from the meteoric water line is interpreted to be caused by the enrichment in ^{18}O by evaporative distillation of geothermal water from an initial $\delta^{18}O_{water}$ around $-25‰$ (see text for details). The blue area highlighted on the meteoric water line represents the range of modern ice and snow from the McMurdo Ice Shelf [*Kellogg et al.*, 1991; *Fitzsimons et al.*, 2012].

interpretation appears to disagree with our conclusion that the prevailing conditions were similar; that is, the change from polar to subpolar conditions at AND-1B was roughly contemporaneous and in agreement with the change in oxygen isotopes at Minna Bluff (Figure 10). However, our results do not preclude a difference in base conditions for glacial ice but suggest only that the climate in this region changed uniformly, as would be expected given the proximity and moderate paleoelevation difference ($\leq$1000 m) between these two areas. We interpret the warmer basal conditions described by *Smellie et al.* [2014] as a consequence of high local heat flow associated with the Minna Bluff magmatic system. The influence of recent subglacial volcanic activity on ice flow in Marie Byrd Land, West Antarctica, has also been used to infer wet-based conditions in a polar environment [*Blankenship et al.*, 1993; *Corr and Vaughan*, 2008; *Lough et al.*, 2013] and has important implications for glacial modeling and climate history.

Our use of carbonate oxygen isotopes from volcanic deposits as a geochemical proxy for paleoclimate is exploratory. But we consider the results presented here to be intriguing and warrant further evaluation and possible application in Antarctica and elsewhere. The fundamental criteria that are necessary to help substantiate the use of this technique include (1) terrestrial glaciovolcanic sequences that preserved lithofacies and architecture to reconstruct ice thickness and extent at the time of volcanism, (2) authigenic carbonates in volcanoclastic deposits that were formed during or soon after deposition, (3) high-precision dates to constrain the age of those deposits, and (4) reliable carbonate formation temperatures. Limitations and uncertainties for each criterion have been discussed in this paper, however, inherent in the first is the assumption that the ice melted during eruption and alteration is in equilibrium with the contemporaneous climate. Hence the melting of older ice, such as that found at the base of thick continental ice sheets, may yield information on paleoclimate but not necessarily for the time period determined by the eruption age.

6. Conclusions

Secondary minerals formed in hyaloclastites and volcaniclastic sediments are used to reconstruct physiochemical conditions of alteration and interpret paleoenvironments synchronous with volcanic activity at Minna Bluff, Antarctica, between 12 and 7 Ma. From this study we have drawn the following main conclusions:

1. Secondary minerals were precipitated within open spaces (e.g., vesicles, vugs, fractures, interclast voids) by fluids during or soon after the formation of volcaniclastic deposits. The alteration of each deposit is considered to have occurred as an isolated, short-term hydrothermal episode with heat and water supplied either directly during the quenching and granulation of magmas (i.e., hyaloclastites) or by newly erupted volcanic material emplaced in close proximity to wet sediments.

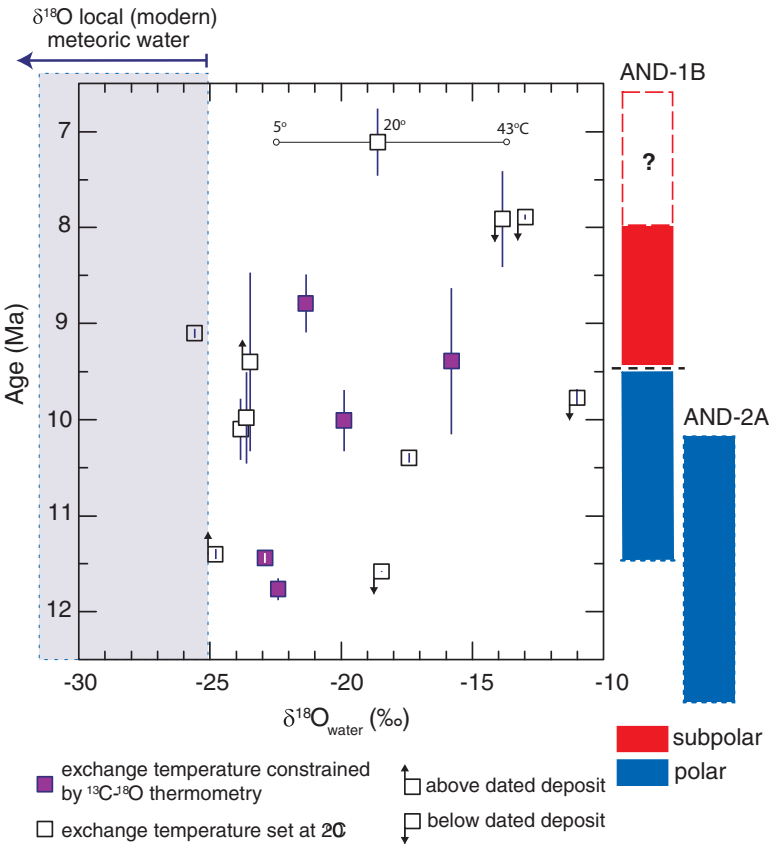

Figure 10. Calculated $\delta^{18}O$ of water for carbonates versus age. The maroon squares represent samples that have temperatures of exchange determined by ^{13}C-^{18}O "clumped isotope" thermometry and the open squares represent water values calculated at 20°C; the median value for the range of temperatures (Δ_{47} = 5 to 43°C) measured by ^{13}C-^{18}O thermometry. The range of modern, local meteoric water values (−25 to −38‰) [*Kellogg et al*., 1991; *Fitzsimons et al*., 2012] are delimited by the shaded area. The ages of the volcaniclastic deposits are based on $^{40}Ar/^{39}Ar$ geochronology [*Fargo*, 2009; *Wilch et al*., 2011; Ross et al., manuscripts in preparation, 2014] (Table 1). Sample ages are either dates that were measured directly from the deposits (n = 6), or bracketed between dated overlying and underlying deposits (n = 4), or based on the age of deposits situated either above or below a dated deposit (n = 6). Error bars are determined for 1σ. Note that for many of the samples the error bars lie within the box symbol. Variations in glacial thermal regime and climate (i.e., polar, frozen based versus subpolar, thawed based) over the period of time that the deposits were formed at Minna Bluff are based on information derived from sedimentary sequences recovered from nearby drill cores (AND-1B [*McKay et al*., 2009] and AND-2A [*Passchier et al*., 2011]).

2. Secondary minerals consist of zeolites most often followed, paragenetically, by carbonates. Zeolites display radial (phillipsite) and pseudocubic to rhombohedral (chabazite) morphologies and strongly alkaline [(Na + K)/Ca >10] compositions similar to zeolites found within closed hydrological systems. Carbonates consist of calcite, low and high Mg-calcite, dolomite, and magnesite, and are compositionally similar to those found in active volcanic-hydrothermal systems.

3. The secondary mineral assemblages at Minna Bluff indicate formation by low-temperature hydrothermal activity (≤200°C). Temperatures based on quartz-calcite equilibrium and carbonate ^{13}C-^{18}O thermometry support a range between 5 and 100°C.

4. Oxygen isotopes measured on carbonates show a wide range of values ($\delta^{18}O$ = −0.50 to 21.53‰) with extremely light calculated $\delta^{18}O_{water}$ (−15.8 to −22.9‰). Hydrogen isotopes measured on opaline silica (δD = −187.8 to −210.4‰) are also extremely light, and along with a mean carbonate $^{87}Sr/^{86}Sr$ ratio of 0.70327 (±0.0009), signify that the parent fluids were derived from ^{18}O-depleted and δD-depleted Antarctic waters without seawater influence.

5. Field and compositional evidence lead us to conclude that the alteration involved rapid and dynamic changes in the physical and chemical conditions associated with episodic volcanic activity in a terrestrial environment where water was readily available but of finite supply (e.g., melting of thin, local ice caps or snowfields).

6. We propose that secondary minerals precipitated during or soon after formation of volcaniclastic deposits in volcanically active areas can provide important information on past climates. Evidence based on the $\delta^{18}O$ of carbonates suggests a warming climate during the eruptive growth of Minna Bluff between 12 and 7 Ma, which is supported by studies on nearby sediment cores (AND-1B and AND-2A).

Acknowledgments

We would like to thank John Farver and Jeff Snyder (BGSU thesis committee) for contributing their time, effort, and expertise to this project. We would also like to thank David Mogk for the use of his lab and hospitality at Montana State University and Lora Wingate for technical guidance at the University of Michigan. We are grateful to two anonymous reviewers for their useful and constructive comments and for editorial handling by Cin-Ty Lee. This research was funded by a collaborative grant NSF OPP 05-38033. It also was supported by UNED/NSF 250550001146, NSF grants EAR-0949191, ARC-1215551, EAR-1325054, EAR-1352212, EAR-1049351, ACS grant 51182-DNI2, DOE grants DE-FG02-13ER16402, and DE-SC0010288, a Hellman Fellowship, and a Katzner grant (BGSU). Data supporting Figure 4 are available in Table S1 of supporting information and data supporting Figure 7 are available in Table S2 of supporting information.

References

Acton, G., et al. (2009), Preliminary integrated chronostratigraphy of the AND-2A Core, ANDRILL Southern McMurdo Sound Project, Antarctica, *Terra Antarct.*, *15*(1), 211–220.

Antibus, J. V. (2012), A petrographic, geochemical and isotopic (Sr, O, H and C) investigation of alteration minerals in volcaniclastic rocks at Minna Bluff, Antarctica: Petrogenesis and implications for paleoenvironmental conditions, MS thesis, 272 pp., Dep. of Geol., Bowling Green State Univ., Bowling Green, Ohio.

Apps, J. A. (1983), Hydrothermal evolution of repository groundwaters in basalt, in *NRC Nuclear Waste Geochemistry '83, U.S. Nucl. Regul. Comm. Rep. NUREG/CP-0052*, U.S. Govt. Print. Off., pp. 14–51.

Barbieri, M., and M. Morotti (2003), Hydrogeochemistry and strontium isotopes of spring and mineral waters from Monte Vulture volcano, Italy, *Appl. Geochem.*, *1*, 117–125, doi:10.1016/S0883-2927(02)00069-08.

Barnaby, R. J., and J. D. Rimstidt (1989), Redox conditions of calcite cementation interpreted from Mn and Fe contents of authigenic calcite, *Geol. Soc. Am. Bull.*, *101*, 795–804.

Barth-Wirsching, U., and H. Höller (1989), Experimental studies on zeolite formation conditions, *Eur. J. Mineral.*, *1*, 489–506.

Best, J. L., C. R. Fielding, I. Jarvis, and P. Mozley (2000), Millenium reviews, *Sedimentology*, *47*, suppl. 1, 1–256.

Bindeman, I. N. (2008), Oxygen isotopes in mantle and crustal magmas as revealed by single crystal analysis, *Rev. Mineral. Geochem.*, *69*, 445–478, doi:10.1130/GES00952.1.

Bindeman, I. N., V. Kamenetsky, J. Palandri, and T. Vennemann (2012), Hydrogen and oxygen isotope behavior during variable degrees of upper mantle melting: Example from the basaltic glasses from Macquarie Island, *Chem. Geol.*, *310–311*, 126–136, doi:10.1016/j.chemgeo.2012.03.031.

Bindeman, I. N., N. Serebryakov, A. Schmitt, J. Vazquez, Y. Guan, B. Astafiev, J. Palandri, and L. Dobrzhinetskaya (2014), Field and microanalytical isotopic investigation of ultra-depleted in 18-O Paleoproterozoic "Slushball Earth" rocks from Karelia, Russia, *Geosphere*, *952*, 1–32, doi:10.1130/GES00952.1.

Bishop, J. L., P. Schiffman, and R. Southhard (2002), Geochemical and mineralogical analysis of palagonite tuffs and altered rinds of pillow basalts in Iceland and applications to Mars, in *Volcano-Ice Interactions on Earth and Mars*, edited by J. L. Smellie and M. G. Chapman, *Geol. Soc. Spec. Publ.*, *202*, 371–392.

Blankenship, D. D., R. E. Bell, S. M. Hodge, J. M. Brozena, J. C. Behrendt, and C. A. Finn (1993), Active volcanism beneath the West Antarctic ice sheet and implications for ice-sheet stability, *Nature*, *362*, 526–529.

Blattner, P. (1985), Isotope shift data and the natural evolution of geothermal systems, *Chem. Geol.*, *49*, 187–203.

Böhlke, J. K., J. Honnorez, and B.-M. Honnorez-Guerstein (1980), Alteration of Basalts from Site 396B, DSDP: Petrographic and mineralogic studies, *Contrib. Mineral. Petrol.*, *73*, 341–364.

Boschi, C., A. Dini, L. Dallai, G. Ruggieri, and G. Gianelli (2009), Enhanced CO_2-mineral sequestration by cyclic hydraulic fracturing and Si-rich fluid infiltration into serpentinites at Malentrata (Tuscany, Italy), *Chem. Geol.*, *265*, 209–226, doi:10.1016/j.chemgeo.2009.03.016.

Böttcher, M. E. (1994), $^{13}C/^{12}C$ and $^{18}O/^{16}O$ fractionation during synthesis of BaMg (CO3)2 and PbMg (CO_3)2, Abstract, International Mineralogical Association, 16th General Meeting, 53, Pisa, Italy.

Carpenter, A. B., and T. W. Oglesby (1976), A model for the formation of luminescently zoned calcite cements and its implications, *Geol. Soc. Am. Abstr. Programs*, *8*, 469–470.

Carpenter, S. J., K. C. Lohmann, P. Holden, L. M. Walter, T. J. Huston, and A. N. Halliday (1991), $\delta^{18}O$ values, $^{87}Sr/^{86}Sr$ and Sr/Mg ratios of Late Devonian abiotic marine calcite: Implications for the composition of ancient seawater, *Geochim. Cosmochim. Acta*, *55*, 1991–2010.

Coombs, D. S., et al. (1997), Recommended nomenclature for zeolite minerals: Report of the subcommittee on Zeolites of the International Mineralogical Association, Commission on New Minerals and Mineral Names, *Can. Mineral.*, *35*, 1571–1606.

Corr, H. F., and D. G. Vaughan (2008), A recent volcanic eruption beneath the West Antarctic Ice sheet, *Nat. Geosci.*, *1*, 122–125, doi:10.1038/ngeo106.

Dallai, L., and R. Burgess (2011), A record of Antarctic surface temperatures between 25 and 50 m.y. ago, *Geology*, *39*(5), 423–426, doi:10.1130/G31569.1.

Deer, W. A., R. A. Howie, and J. Zussman (1966), *An Introduction to the Rock-Forming Minerals*, John Wiley, N. Y.

Dennis, K. J., H. P. Affek, B. H. Passey, D. P. Schrag, and J. M. Eiler (2011), Defining an absolute reference frame for "clumped" isotope studies of CO_2, *Geochim. Cosmochim. Acta*, *75*(22), 7117–7131, doi:10.1016/j.gca.2011.09.025.

Dennison, R. E., W. Kirkland, and R. Evans (1998), Using Strontium isotopes to determine the age and origin of gypsum and anhydrite beds, *J. Geol.*, *106*(1), 1–18.

Denton, G. H., and D. R. Marchant (2000), The geologic basis for a reconstruction of an ice sheet in McMurdo Sound, Antarctica, at the Last Glacial Maximum, *Geogr. Ann., Ser. A*, *82*, 167–211.

Destrigneville, C., J. Schott, Y. Caristan, and P. Agrinier (1991), Evidence of an early alteration process driven by magmatic fluid in Mururoa volcano, *Earth Planet. Sci. Lett.*, *104*, 119–139.

Di Vincenzo, G., L. Bracciali, P. Del Carlo, K. Panter, and S. Rocchi (2009), $^{40}Ar–^{39}Ar$ dating of volcanogenic products from the AND-2A core (ANDRILL Southern McMurdo Sound Project, Antarctica): Correlations with the Erebus Volcanic Province and implications for the age model of the core, *Bull. Volcanol.*, *72*(4), 487–505.

Dunbar, N. W., K. S. Panter, M. Scanlon, A. J., Fargo, W. C. McIntosh, and T. I. Wilch (2008), Petrology of inclusion rich lavas at Minna Bluff, Antarctica: TI: Evidence for complex mixing processes controlling the composition of a wide range of alkaline volcanic rocks at Minna Bluff, *Eos Trans. AGU*, *89*(53), Fall Meet. Suppl., Abstract V13C-2128.

Ehrenberg, S. N., P. Aagaard, M. J. Wilson, A. R. Fraser, and D. M. L. Duthie (1993), Depth-dependent transformation of kaolinite to dickite in sandstones of the Norwegian continental shelf, *Clay Miner.*, *28*(3), 525–552.

Eiler, J. M. (2007), "Clumped-isotope" geochemistry: The study of naturally-occurring, multiple substituted isotopologues, *Earth Planet. Lett.*, *262*, 309–327.

Fargo, A. F. (2009), 40Ar/39Ar geochronological analysis of Minna Bluff, Antarctica: Evidence for past glacial events within the Ross Embayment, MS thesis, 48 pp., N. M. Inst. of Mining and Technol., Socorro.
Faure, G., and T. M. Mensing (2005), *Isotopes: Principles and Application*, John Wiley, N. Y.
Feakins, S. J., S. Warny, and J. E. Lee (2012), Hydrologic cycling over Antarctica during the middle Miocene warming, *Nat. Geosci.*, *5*, 557–560, doi:10.1038/NGEO1498.
Fisher, R., and A. M. Stueber (1976), Strontium isotopes in selected streams within the Susquehanna River basin, *Water Resour. Res.*, *12*, 1061–1068.
Fisher, R. V., and H.-U. Schmincke (1984), *Pyroclastic Rocks*, Springer, N. Y.
Fitzsimons, S., S. Mager, R. Frew, A. Clifford, and G. Wilson (2012), Formation of ice-shelf moraines by accretion of sea water and marine sediment at the southern margin of the McMurdo Ice Shelf, Antarctica, *Ann. Glaciol.*, *53*(60), 211–220, doi:10.3189/2012AoG60A155.
Flügel, E. (2010), *Microfacies of Carbonate Rocks: Analysis, Interpretation and Application*, 2nd ed., Springer, N. Y.
Friedman, I., and J. R. O'Neil (1977), Compilation of stable isotope fractionation factors of geochemical interest, in *Compilation of Geochemistry*, 6th ed., edited by M. Fleischer, *U.S. Geol. Surv. Prof. Pap.*, U.S. Govt. Print. Off., *440-KK*, 12 pp.
Geldmacher, J., and K. Hoernle (2000), The 72 Ma geochemical evolution of the Madeira hotspot (eastern North Atlantic): recycling of Paleozoic ($\leq$ 500 Ma) oceanic lithosphere, Earth and Planetary Science Letters, *183*, pp. 73–92.
Ghosh, P., J. Adkins, H. Affek, B. Balta, W. F. Guo, E. A. Schauble, D. Schrag, and J. M. Eiler (2006), ^{13}C–^{18}O bonds in carbonate minerals: A new kind of paleothermometer, *Geochim. Cosmochim. Acta*, *70*(6), 1439–1456, doi:10.1016/j.gca.2005.11.014.
Graham, I. T., R. E. Pogson, D. M. Colchester, and A. Baines (2003), Zeolite crystal habits, compositions and paragenesis: Blackhead Quarry, Dunedin, New Zealand, *Mineral. Mag.*, *67*(4), 625–627, doi:10.1180/0026461036740122.
Greenberger, R. N., J. F. Mustard, P. S. Kumar, M. D. Dyar, E. A. Breves, and E. C. Sklute (2012), Low temperature aqueous alteration of basalt: Mineral assemblages of Deccan basalts and implications for Mars, *J. Geophys. Res.*, *117*, E00J12, doi:10.1029/2012JE004127.
Gysi, A. P., and A. Stefánsson (2012), Mineralogical aspects of CO_2 sequestration during hydrothermal basalt alteration—An experimental study at 75 to 250°C and elevated pCO_2, *Chem. Geol.*, *306–307*, 146–159, doi:10.1016/j.gca.2005.11.014.
Hammer, Ø., and D. Harper (2006), *Paleotological Data Analysis*, Blackwell, Malden, Mass.
Hay, R. L. (1964), Phillipsite of saline lakes and soils, *Am. Mineral.*, *49*, 1366–1387.
Hay, R. L. (1966), Zeolites and zeolitic reactions in sedimentary rocks, *Geol. Soc. Am. Spec. Pap.*, *85*, 1–130.
Hay, R. L. (1978), Geologic occurrence of zeolites, in *Natural Zeolites: Occurrence, Properties, Use*, edited by L. B. Sand and F. A. Mumpton, pp. 135–144, Pergamon, Oxford, U. K.
Herrero, M. J., A. Martín-Pérez, A. M. Alonso-Zarza, I. Gil-Peña, A. Meléndez, and R. Martín-García (2011), Petrography and geochemistry of the magnesites and dolostones of the Ediacaran Ibor Group (635 to 542 Ma), Western Spain: Evidences of their hydrothermal origin, *Sediment. Geol.*, *240*, 71–84, doi:10.1016/j.sedgeo.2011.08.00.7.
Horbury, A. D., and A. E. Adams (1989), Meteoric phreatic diagenesis in cyclic late Dinantian carbonates, northwest England, *Sediment. Geol.*, *65*, 319–344.
Huntington, K. W., et al. (2009), Methods and limitations of "clumped" CO_2 isotope (D47) analysis by gas-source isotope-ratio mass spectrometry, *J. Mass Spectrom.*, *44*, 1318–1329, doi:10.1002/jms.1614.
Ibrahim, K. (2004), Mineralogy and chemistry of natrolite from Jordan, *Clay Miner.*, *39*(1), 47–55, doi:10.1180/0009855043910119.
Jackson, M. G., and S. R. Hart (2006), Strontium isotopes in melt inclusions from Samoan basalts: Implications for heterogeneity in the Samoan plume, *Earth Planet. Sci. Lett.*, *245*, 260–277, doi:10.1016/j.epsl.2006.02.040.
Jakobsson, S.P., M.T. Gudmundsson (2012), Móbergsmyndunin og gos undir jöklum. (In Icelandic with English summary: The Moberg formation and subglacial volcanic eruptions), *Náttúrufræöingurinn 82*, 113–125.
Jakobsson, S. P., and M. T. Gudmundsson (2008), Subglacial and intraglacial volcanic formations in Iceland, *Jökull*, *58*, 179–196.
Jakobsson, S. P., and J. G. Moore (1986), Hydrothermal minerals and alteration rates at Surtsey volcano, Iceland, *Geol. Soc. Am. Bull.*, *97*, 648–659.
Johnson, J. S., and J. L. Smellie (2007), Zeolite compositions as proxies for eruptive paleoenvironment, *Geochem. Geophys. Geosyst.*, *8*, Q03009, doi:10.1029/2006GC001450.
Kawabe, I. (1979), Lattice dynamical aspect of oxygen isotope partition function ratio for alpha quartz, *Geochem. J.*, *13*(2), 57–67, doi:10.2343/geochemj.13.57.
Kellogg, T. B., D. E. Kellogg, and M. Stuiver (1991), Oxygen isotope data from the McMurdo Ice Shelf, Antarctica: Implications for debris band formation and glacial history, *Antarct. J. U. S.*, *26*, 73–76.
Kelly, P. J., P. Kyle, and N. W. Dunbar (2006), Crystallization processes and magma chamber dynamics at the Mount Erebus Volcano Lava Lake: The mineralogic message, *Eos Trans. AGU*, *87*(52), Fall Meet. Suppl., Abstract V53E-04.
Kónya, P., and S. Szakáll (2011), Occurrence, composition and paragenesis of the zeolites and associated minerals in the alkaline basalt of a maar-type volcano at Haláp Hill, Balaton Highland, Hungary, *Mineral. Mag.*, *75*(6), 2869–2885, doi:10.1180/minmag.2011.075.6.2869.
Kralik, M., P. Ahron, E. Schroll, and V. Zachmann (1989), Carbon and oxygen isotope systematics of magnesites in magnesite formation, *Monogr. Ser. Miner. Deposits*, *28*, 207–224.
Kristmannsdottir, H., and J. Tomasson (1978), Zeolite zones in geothermal areas in Iceland, in *Natural Zeolites: Occurrence, Properties, Use*, edited by L. B. Sand and F. A. Mumpton, pp. 277–284, Pergamon, N. Y.
Kyle, P. R. (1981), Mineralogy and geochemistry of a basanite to phonolite sequence at Hut Point Peninsula, Antarctica, based on core from Dry Valley Drilling Project Drillholes 1, 2 and 3, *J. Petrol.*, *22*, 451–500, doi:10.1093/petrology/22.4.451.
Kyle, P. R. (1990), Erebus Volcanic Province, in *Volcanoes of the Antarctic Plate and Southern Oceans*, vol. 48, edited by W. E. LeMasurier and J. W. Thomson, pp. 81–145, AGU, Washington, D. C.
Kyle, P. R., J. A. Moore, and M. F. Thirlwall (1992), Petrologic evolution of anorthoclase phonolite lavas at Mount Erebus, Ross Island, Antarctica, *J. Petrol.*, *33*, 849–875.
Larsen, D. (2008), Revisiting silicate authigenesis in the Pliocene–Pleistocene Lake Tecopa beds, southeastern California: Depositional and hydrological controls, *Geosphere*, *152*(1), 612–639, doi:10.1130/GES00152.1.
Lewis, A. R., D. R. Marchant, A. C. Ashworth, S. R. Hemming, and M. L. Machlus (2007), Major middle Miocene global climate change: Evidence from East Antarctica and the Transantarctic Mountains, *Geol. Soc. Am. Bull.*, *119*, 1449–1461, doi:10.1130/B26134.
Lough, A. C., D. A. Wiens, C. G. Barcheck, S. Anandakrishnan, R. C. Aster, D. D. Blankenship, A. D. Huerta, A. Nyblade, D. A. Young, and T. J. Wilson (2013), Seismic detection of an active subglacial magmatic complex in Marie Byrd Land, Antarctica, *Nat. Geosci.*, *6*(12), 1031–1035, doi:10.1038/ngeo1992.
Major, R. P., and R. J. Wilber (1991), Crystal habit, geochemistry, and cathodoluminescence of magnesian calcite marine cements from the lower slope of Little Bahama Bank, *Geol. Soc. Am. Bull.*, *103*, 461–471.

Marcano, M. C., S. Mukasa, K. C. Lohmann, C. Stefano, M. Tavianiand, and A. Andronikov (2009), Chronostratigraphic and paleoenvironmental constraints derived from the $^{87}Sr/^{86}Sr$ and $\delta^{18}O$ signal of Miocene bivalves, southern McMurdo Sound, Antarctica, *Global Planet. Change*, *69*, 124–132, doi:10.1016/j.gloplacha.2009.05.001.

Marks, N., P. Schiffman, R. A. Zierenberg, H. Franzson, and G. Ó. Fridleifsson (2010), Hydrothermal alteration in the Reykjanes geothermal system: Insights from Iceland deep drilling program well RN-17, *J. Volcanol. Geotherm. Res.*, *189*, 172–190, doi: 10.1016%2Fj.jvolgeores.2009.10.018.

Martin, A. P., A. F. Cooper, and R. C. Price (2013), Petrogenesis of Cenozoic, alkali volcanic lineages at Mount Morning, West Antarctica and their entrained lithospheric mantel xenoliths: Lithospheric versus asthenospheric mantle sources, *Geochim. Cosmochim. Acta*, *122*, 127–152, doi:10.1016/j.gca.2013.08.025.

Masson-Delmotte, V., et al. (2008), A review of Antarctic surface snow isotopic composition: Observations, atmospheric circulation, and isotopic modeling, *J. Clim.*, *21*, 3359–3387, doi:10.1175/2007JCLI2139.1.

McKay, R., et al. (2009), The stratigraphic signature of the late Cenozoic Antarctic Ice Sheets in the Ross Embayment, *Geol. Soc. Am. Bull.*, *121*(11/12), 1537–1561, doi:10.1130/B26540.1.

Morteani, G., Y. Kostitsyn, C. Preinfalk, and H. A. Gilg (2010), The genesis of the amethyst geodes at Artigas (Uruguay) and the paleohydrology of the Guarani aquifer: Structural, geochemical, oxygen, carbon, strontium isotope and fluid inclusion study, *Int. J. Earth Sci.*, *99*, 927–947, doi:10.1007/s00531-009-0439-z.

Naish, T., et al. (2009), Obliquity-paced Pliocene West Antarctic ice sheet oscillations, *Nature*, *458*, 322–328, doi:10.1038/nature07867.

O'Neil, J. R., R. N. Clayton, and T. K. Mayeda (1969), Oxygen isotope fractionation in divalent metal carbonates, *J. Chem. Phys. 51*, pp. 5547–5558.

Oppenheimer, C., R. Moretti, P. R. Kyle, A. Eschenbacher, J. B. Lowenstern, R. L. Hervig, and N. W. Dunbar (2011), Mantle to surface degassing of alkali magmas at Erebus volcano, Antarctica, *Earth Planet. Sci. Lett.*, *306*, 261–271.

Panter, K. S., J. Blusztajn, D. Wingrove, S. Hart, D. Mattey, (2003), Sr, Nd, Pb, Os, O isotope, Major and trace element data from basalts, South Victoria Land, Antarctica: Evidence for open-system processes in the evolution of mafic alkaline magmas. *General Assembly of the European Geosciences Union, Geophys. Res. Abst*, v. 5, 07583.

Panter, K. S., N. Dunbar, M. Scanlan, T. I. Wilch, A. Fargo, and W. McIntosh (2011), Petrogenesis of alkaline magmas at Minna Bluff, Antarctica: Evidence for multi-stage differentiation and complex mixing processes, Abstract V31f-2590 presented at the 2011 Fall Meeting, AGU, San Francisco, Calif., 5–9 Dec.

Passaglia, E., G. Vezzalini, and R. Carnevali (1990), Diagenetic cabazite and phillipsites in Italy: Crystal chemistry and genesis, *Eur. J. Mineral.*, *2*, 827–839.

Passchier, S., G. Browne, B. Field, C. R. Fielding, L. A. Krissek, K. Panter, S. F. Pekar, and ANDRILL-SMS Science Team (2011), Early and Middle Miocene Antarctic glacial history from the sedimentary facies distribution in the AND-2A drill hole, Ross Sea, Antarctica, *Geol. Soc. Am. Bull.*, *123*(11–12), 2352–2365, doi:10.1130/B30334.1.

Renac, C., K. Kyser, P. Bowden, B. Moine, and J.-Y. Cottin (2010), Hydrothermal fluid interaction in basaltic lava units, Kerguelen Archipelago (SW Indian Ocean), *Eur. J. Mineral.*, *22*, 215–234, doi:10.11270935-1221/2009/0022-1993.

Révillon, S., D. A. H. Teagle, P. Boulvais, J. Shafer, and C. R. Neal (2007), Geochemical fluxes related to alteration of a subaerially exposed seamount: Nintoku seamount, ODP Leg 197, Site 1205, *Geochem. Geophys. Geosyst.*, *8*, Q02014, doi:10.1029/2006GC001400.

Reyes, A. G. (1990), Petrology of Philippine geothermal systems and the application of alteration mineralogy to their assessment, *J. Volcanol. Geotherm. Res.*, *43*, 279–309.

Rilling, S., S. Mukasa, T. Wilson, L. Lawyer, and C. Hall (2009), New determinations of 40Ar/39Ar isotopic ages and flow volumes for Cenozoic volcanism in the Terror Rift, Ross Sea, Antarctica, *J. Geophys. Res.*, *114*, B12207, doi:10.1029/2009JB006303.

Scanlan, M., K. S. Panter, T. I. Wilch, N. W. Dunbar, and W. C. McIntosh (2008), Petrology of inclusion-rich lavas at Minna Bluff, Antarctica: Implications for magma origin, differentiation and eruption dynamics, *Eos Trans. AGU*, *89*(53), Fall Meet. Suppl., Abstract V13C-2129.

Schroll, E. (2002), Genesis of magnesite deposits in the view of isotope geochemistry, *Bol. Paranaense Geocienc.*, *50*, 59–68.

Scott, G. L. (2004), Major active faults determine the location of the Tongonan geothermal field: Evidence provided by rock alteration and stable isotope geochemistry, *Isl. Arc*, *13*, 370–386, doi:10.1111/j.1440–1738.2004.00432.x.

Shah, M. M., F. H. Nader, D. Garcia, R. Swennen, and R. Ellam (2012), Hydrothermal dolomites in the Early Albian (Cretaceous) platform carbonates (NW Spain): Nature and origin of dolomites and dolomitising fluids, oil & gas science and technology, *Rev. IFP Energies Nouvelles*, *67*(1), 97–122, doi:10.2516/ogst/2011174.

Sharma, S., D. J. Patil, and K. Gopalan (2002), Temperature dependence of oxygen isotope fractionation of CO_2 from magnesite-phosphoric acid reaction, *Geochim. Cosmochim. Acta*, *66*, 589–593, doi:10.1016/S0016-7037(01)00833-X.

Sharp, Z. D., and D. L. Kirschner (1994), Quartz-calcite oxygen isotope thermometry: A calibration based on natural isotopic variations, *Geochim. Cosmochim. Acta*, *58*, 4491–4501, doi:10.1016%2F0016-7037%2894%2990350-6.

Sheppard, R. A., and J. J. Fitzpatrick (1989), Phillipsite from silicic tuffs in saline, alkaline-lake deposits, *Clays Clay Miner.*, *37*(3), 243–247, doi: 10.1346%2FCCMN.1989.0370307.

Sims, K. W. W., J. Blichert-Toft, P. R. Kyle, S. Pichat, P.-J. Gauthier, J. Blusztajn, P. Kelly, L. Ball, and G. Layne (2008), A Sr, Nd, Hf, and Pb isotope perspective on the genesis and long-term evolution of alkaline magmas from Erebus volcano, Antarctica, *J. Volcanol. Geotherm. Res.*, *177*, 606–618, doi:10.1016/j.jvolgeores.2007.08.006.

Smellie, J. L. (2000), Subglacial eruptions, in *Encyclopedia of Volcanoes*, edited by H. Sigurdsson, pp. 403–430, Academic, San Diego, Calif.

Smellie, J. L., T. I. Wilch, and S. Rocchi (2013), 'A' ā, lava-fed deltas: A new reference tool in paleoenvironmental studies, *Geology*, *41*, 403–407, doi:10.1130/G33631.1.

Smellie, J. L., S. Rocchi, T. I. Wilch, M. Gemelli, G. Di Vincenzo, W. McIntosh, N. Dunbar, K. Panter, and A. Fargo (2014), Glaciovolcanic evidence for a polythermal Neogene East Antarctic Ice Sheet, *Geology*, *42*, 39–41, doi:10.1130/G34787.1.

Staudigel, H., G. R. Davies, S. R. Hart, K. M. Marchant, and B. M. Smith (1995), Large-scale isotopic Sr, Nd and O isotopic anatomy of altered oceanic-crust—DSDP/ODP sites 417/418, *Earth Planet. Sci. Lett.*, *130*(1–4), 169–185.

Stewart, M. K. (1975), Hydrogen and oxygen isotope studies on the McMurdo ice shelf, Antarctica, *N. Z. J. Geol. Geophys.*, *18*, 49–64.

Stroncik, N. A., and H.-U. Schmincke (2002), Palagonite—A review, *Int. J. Earth Sci.*, *91*, 680–697, doi:10.1007/s00531-001-0238-7.

Surdam, R. C., and H. P. Eugster (1976), Mineral reactions in the sedimentary deposits of the Lake Magadi region, Kenya, *Geol. Soc. Am. Bull.*, *87*, 1739–1752.

Surdam, R. C., and R. A. Shepphard (1978), Zeolites in saline, alkaline lake deposits, in *Natural Zeolites: Occurrences, Properties, Use*, edited by L. B. Sand and F. A. Mumpton, pp. 145–174, Pergamon, Oxford, U. K.

Talarico, F., and S. Sandroni (2009), Provenance signatures of the Antarctic Ice Sheets in the Ross Embayment during the Late Miocene to Early Pliocene: The ANDRILL AND-1B core record, *Global Planet. Change*, *69*, 103–123, doi:10.1016/j.gloplacha.2009.04.007.

Taylor, H. P., Jr. (1977), Water/rock interactions and the origin of H_2O in granitic batholiths, *J. Geol. Soc. London*, *133*, 509–558.
Tucker M. E, Wright P. V. (1990), Carbonate Sedimentology, 482 p., Blackwell, Oxford, U. K.
Tripati, A., N. Thiagarajan, R. Eagle, A. Gagnon, H. Bauch, J. Eiler (2010), Apparent equilibrium ^{13}C-^{18}O isotope signatures and 'clumped isotope' thermometry in foraminifera and coccoliths, Geochimica et Cosmochimica Acta, *74*, pp. 5697–5717.
Walton, A. W., and P. Schiffman (2003), Alteration of hyaloclastites in the HSDP 2 phase 1 drill core: 1. Description and paragenesis, *Geochem. Geophys. Geosyst.*, *4*(5), 8709, doi:10.1029/2002GC000368.
Walton, A. W., P. Schiffman, and G. L. Macpherson (2005), Alteration of hyaloclastites in the HSDP 2 Phase 1 Drill Core: 2. Mass balance of the conversion of sideromelane to palagonite and chabazite, *Geochem. Geophys. Geosyst.*, *6*, Q09G19, doi:10.1029/2004GC000903.
Wardell, L. J., P. R. Kyle, and C. Chaffin (2004), Carbon dioxide and caron monoxide emission rates from an alkaline intra-plate volcano: Mt. Erebus, Antarctica, *J. Volcanol. Geotherm. Res.*, *131*, 109–121.
White, J. D. L., and B. F. Houghton (2006), Primary volcaniclastic rocks, *Geology*, *34*, 677–680, doi:10.1130/G22346.1.
Wilch, T. I., K. S. Panter, W. C. McIntosh, N. W. Dunbar, J. L. Smellie, A. Fargo, J. Ross, J. Antibus, M. Scanlan, M. Zimmerer, (2011), Miocene evolution of the Minna Bluff Volcanic Complex, Ross Embayment, Antarctica. *International Symposium on Antarctic Earth Science XI, Abstract* PS5.10, Edinburgh, Scotland.
Wilson, G. S., et al. (2012), Neogene tectonic and climatic evolution of the Western Ross Sea, Antarctica—Chronology of events from the AND-1B drill hole, *Global Planet. Change*, *96–97*, 189–209, doi:10.1016/j.gloplacha.2012.05.019.
Wilson, T. J., and C. M. Demosthenous (2000), SAR-based mapping of glaciated volcanic terrain: The Erebus Volcanic Province, Antarctica, *Can. J. Remote Sens.*, *26*, 142–158.
Wright-Grassham, A. C. (1987), Volcanic geology, mineralogy and petrogenesis of the Discovery Volcanic Subprovince, southern Victoria Land, Antarctica, PhD dissertation, N. M. Inst. of Mining and Technol., 460 pp., Socorro.